













## PAPER

[View Article Online](#)  
[View Journal](#) | [View Issue](#)Cite this: *Dalton Trans.*, 2025, **54**,  
2340

# Water-soluble platinum and palladium porphyrins with peripheral ethyl phosphonic acid substituents: synthesis, aggregation in solution, and photocatalytic properties†

Marina V. Volostnykh, <sup>a,b</sup> Gayane A. Kirakosyan, <sup>a,c</sup> Anna A. Sinelshchikova, <sup>a,h</sup> Elizaveta V. Ermakova, <sup>a</sup> Yulia G. Gorbunova, <sup>a,c</sup> Aslan Yu. Tsvadze, <sup>a,c</sup> Sergey M. Borisov, <sup>d</sup> Michel Meyer, <sup>b</sup> Lhoussain Khrouz, <sup>e</sup> Cyrille Monnereau, <sup>e</sup> Stephane Parola <sup>f</sup> and Alla Bessmertnykh-Lemeune <sup>\*b,g</sup>

Water-soluble porphyrins have garnered significant attention due to their broad range of applications in biomedicine, catalysis, and material chemistry. In this work, water-soluble platinum(II) and palladium(II) complexes with porphyrins bearing ethyl phosphonate substituents, namely, Pt/Pd 10-(ethoxyhydroxyphosphoryl)-5,15-di(*p*-carboxyphenyl)porphyrins (**M3m**, M = Pt(II), Pd(II)) and Pt/Pd 5,10-bis(ethoxyhydroxyphosphoryl)-10,20-diarylporphyrins (**M1d–M3d**; aryl = *p*-tolyl (**1**), mesityl (**2**), *p*-carboxyphenyl (**3**)), were synthesized by alkaline hydrolysis of the corresponding diethyl phosphonates **M6m** and **M4d–M6d**. NMR, UV–vis, and fluorescence spectroscopy revealed that the mono-phosphonates **M3m** tend to form aggregates in aqueous media, while the bis-phosphonates **M3d** exist predominantly as monomeric species across a wide range of concentrations ( $10^{-6}$ – $10^{-3}$  M), ionic strengths (0–0.81 M), and pH values (4–12). Single-crystal X-ray diffraction studies of the diethyl phosphonates **Pt6d** and **Pd6d** revealed that  $\pi$ – $\pi$  stacking of the aromatic macrocycles is sterically hindered in the crystals, providing a rationale for the low degree of solution aggregation observed for ethyl phosphonate **M3d**. Photophysical studies of **M3m** and **M1d–M3d** demonstrated that these compounds are phosphorescent and generate singlet oxygen in aqueous solutions. Pd(II) complex **Pd3d** is an excellent photocatalyst for the oxidation of sulfides using dioxygen in a solvent mixture (MeCN/H<sub>2</sub>O, 4 : 1 v/v). Under these conditions, various alkyl and aryl sulfides were quantitatively converted into the desired sulfoxides. For the oxygenation of mixed alkyl–aryl sulfides, **Pd3d** outperforms Pd(II) meso-tetrakis(*p*-carboxyphenyl)porphyrin (PdTCPP). This photocatalyst can be recycled and reused to afford sulfoxides with no loss of product yield.

Received 1st November 2024,  
Accepted 13th December 2024

DOI: 10.1039/d4dt03068k

[rsc.li/dalton](http://rsc.li/dalton)

## Introduction

Water-soluble porphyrins have garnered enormous attention over the past fifty years. These compounds are extensively studied in biomedicine, serving as photosensitizers (PSs) in photodynamic therapy (PDT)<sup>1,2</sup> and contrast agents in fluorescence-based diagnostic methods,<sup>3</sup> magnetic resonance (MRI),<sup>4</sup> and photoacoustic imaging.<sup>5,6</sup> Many ongoing studies inspired by natural processes focus on utilizing porphyrins as catalysts for hydrogen production, CO<sub>2</sub> reduction, oxidation, C–C bond formation, and chlorination reactions.<sup>7–9</sup> Water-soluble porphyrins enable catalytic reactions to be conducted in aqueous media, similar to natural systems.<sup>10–13</sup> They are also being studied as reusable catalysts in post-synthesis liquid-phase separation processes.<sup>12,14</sup>

In material and supramolecular chemistry, these compounds have been extensively explored for preparing func-

<sup>a</sup>Frumkin Institute of Physical Chemistry and Electrochemistry, Russian Academy of Sciences, Leninsky pr. 31-4, Moscow, 119071, Russia<sup>b</sup>Institut de Chimie Moléculaire de l'Université de Bourgogne (ICMUB), UMR 6302 CNRS, Université de Bourgogne, 9 Avenue Alain Savary, BP 47870 21078 Dijon Cedex, France. E-mail: [alla.lemeune@ens-lyon.fr](mailto:alla.lemeune@ens-lyon.fr)<sup>c</sup>Kurnakov Institute of General and Inorganic Chemistry, Russian Academy of Sciences, Leninsky pr. 31, Moscow, 119991, Russia<sup>d</sup>Institute of Analytical Chemistry and Food Chemistry, Graz University of Technology, Stremayrgasse 9, 8010 Graz, Austria<sup>e</sup>ENS de Lyon, CNRS, LCH, UMR 5182, 69342 Lyon Cedex 07, France<sup>f</sup>UCBL, ENS de Lyon, CNRS, LCH, UMR 5182, 69342 Lyon Cedex 07, France<sup>g</sup>CNRS, ENS de Lyon, LCH, UMR 5182, 69342 Lyon Cedex 07, France<sup>h</sup>BCMaterials, Basque Center for Materials, Applications and Nanostructures, UPV/EHU Science Park, 48940 Leioa, Spain†Electronic supplementary information (ESI) available. CCDC 2027752 and 2027753. For ESI and crystallographic data in CIF or other electronic format see DOI: <https://doi.org/10.1039/d4dt03068k>

tional materials for biomedicine<sup>15–17</sup> and fabricating oxygen-sensitive membranes,<sup>18,19</sup> sensors for volatile organic compounds,<sup>20</sup> and photocatalysts for degradation of environmental pollutants.<sup>21</sup> A<sub>4</sub>-type porphyrins are large molecules with D<sub>4h</sub> symmetry, bearing four peripheral metal-coordinating groups (such as carboxylate, phosphonate, and sulfonate) that serve as excellent precursors for MOFs.<sup>22,23</sup> Their high solubility in polar solvents is a mandatory prerequisite for MOF synthesis, which typically requires homogeneous conditions and must be carried out by using metal salts as reagents. Stable and highly porous porphyrin-based MOFs have already been successfully studied as sensors,<sup>24</sup> proton-conducting materials,<sup>25,26</sup> and catalysts.<sup>27–29</sup>

To make the inherently hydrophobic aromatic tetrapyrrolic macrocycles soluble in aqueous environments, numerous strategies have been developed, such as introducing specific hydrophilic substituents like pyridinium, sulfonate, or carboxylate groups.<sup>30</sup> However, these negatively or positively charged molecules still tend to aggregate in aqueous media, which adversely affects their light absorption, luminescence, and ability to generate singlet oxygen and interact with guest molecules.<sup>31–33</sup> To counteract this aggregation, several approaches have been explored. One strategy involves preparing sterically constrained conjugates with hydrophilic residues like sugar<sup>34,35</sup> or polyethylene glycol (PEG) moieties,<sup>36</sup> or incorporating them into hydrophilic dendrimers.<sup>37</sup> Alternatively, the water solubility of hydrophobic porphyrins can also be enhanced by encapsulating them within cyclodextrin cavities,<sup>38</sup> forming micelles,<sup>39–41</sup> or using other nanoscale organic or inorganic carriers.<sup>42</sup>

Functionalization of tetrapyrrolic macrocycles through the covalent attachment of hydrophilic residues is generally more convenient compared to supramolecular strategies, especially for biochemistry and catalysis. This is largely because supramolecular assemblies are sensitive to environmental factors and may result in unexpected dissociation in reaction media and loss of activity. Unfortunately, there are still considerable synthetic challenges in the functionalization of the tetrapyrrolic macrocycle by hydrophilic groups. Most substituents are commonly introduced at the *meso*-positions of the macrocycle because chemoselective modifications at the  $\beta$ -positions remain difficult to achieve. Additionally, hydrophilic porphyrins are often prepared using hydrophobic 1,4-phenylene linkers since direct sulfonation and carboxylation of the macrocycle itself is not feasible.

Recently, it has been shown that diethyl phosphonate groups can be directly attached to the macrocycle in both the *meso*- and  $\beta$ -positions, affording phosphonate diesters that can be converted into their water-soluble acidic derivatives.<sup>43–46</sup> These substituents allow fine-tuning of the hydrophilic–lipophilic balance of the molecules and also significantly impact the electronic structure of the porphyrin macrocycle because of their direct attachment to the aromatic ring. However, the stability of the C–P bond in these sterically bulky compounds is lower compared to that of traditional phosphonic acid diesters, particularly under acidic conditions. This leads to undesirable cleavage of this bond and

limits the possibilities for their conversion to the target acids, as dialkyl phosphonates are typically transformed into the corresponding acids under acidic conditions. Our previous research has also demonstrated that porphyrins bearing monoalkyl phosphonate groups, which can be synthesized under basic conditions, are also water-soluble and can be obtained from diesters in high yields.<sup>47</sup> To date, only water-soluble Mn(III), In(III), and Ga(III) complexes of this series have been reported.<sup>47,48</sup> In this work, the palladium (Pd(II)) and platinum (Pt(II)) complexes **M3m** and **M1d–M3d** were obtained and investigated (Fig. 1).

Robust Pt/Pd porphyrins and related compounds (such as benzoporphyrins, chlorins, bacteriochlorins, and corroles), which incorporate heavy atoms within the macrocyclic cavity, are well known for their ability to produce long-lived triplet states through an excited-state process called intersystem crossing (ISC) when irradiated with visible light.<sup>49,50</sup> These triplet states are highly susceptible to dynamic quenching by molecular oxygen, making these complexes highly effective for oxygen sensing.<sup>51–54</sup> The generation of reactive oxygen species during this process is used in PDT and photocatalysis.<sup>55,56</sup> Additionally, Pt(II) porphyrins have been studied in the development of oxygen microscopy techniques through two-photon-excited phosphorescence.<sup>57,58</sup> Pd(II) complexes have also been explored in transition-metal (redox) catalysis.<sup>59</sup>

In this work, we disclose the efficient synthesis of ethyl phosphonate and bis(ethyl phosphonate) derivatives **M3m** and **M1d–M3d**, respectively (Fig. 1), their aggregation behavior in solution, their ability to generate singlet oxygen in aqueous media and their photocatalytic properties. Comparative studies of bis-phosphonates **M3d** and palladium and platinum *meso*-tetra(*p*-carboxyphenyl)porphyrins (MTCPP, M = Pt(II), Pd(II)) revealed that the degree of aggregation in aqueous media is significantly lower for compounds with voluminous phosphonate groups, which are deprotonated over a wide pH range (pH > 4). The metalloporphyrins reported in this work are efficient photosensitizers for generating singlet oxygen and can be used for selective photooxidation of sulfides to sulfoxides.

## Results and discussion

### Synthesis of metalloporphyrins

Mono- and bis-phosphonate diesters, **H<sub>2</sub>6m** and **H<sub>2</sub>4d–H<sub>2</sub>6d**, respectively, were prepared using the Pd-catalyzed phosphorylation reaction, following the previously reported procedure.<sup>44,45</sup> The insertion of Pd(II) ions into free-base porphyrins can be performed in aqueous media after transformation of these diesters into the corresponding acids.<sup>16,60</sup> However, in our case, the alkaline hydrolysis of the corresponding complexes with phosphonate diester groups **M6m** and **M4d–M6d** enables a more convenient purification procedure (Scheme 1).

The Pt(II) and Pd(II) complexes **M6m** and **M4d–M6d** were obtained using synthetic procedures recently published by

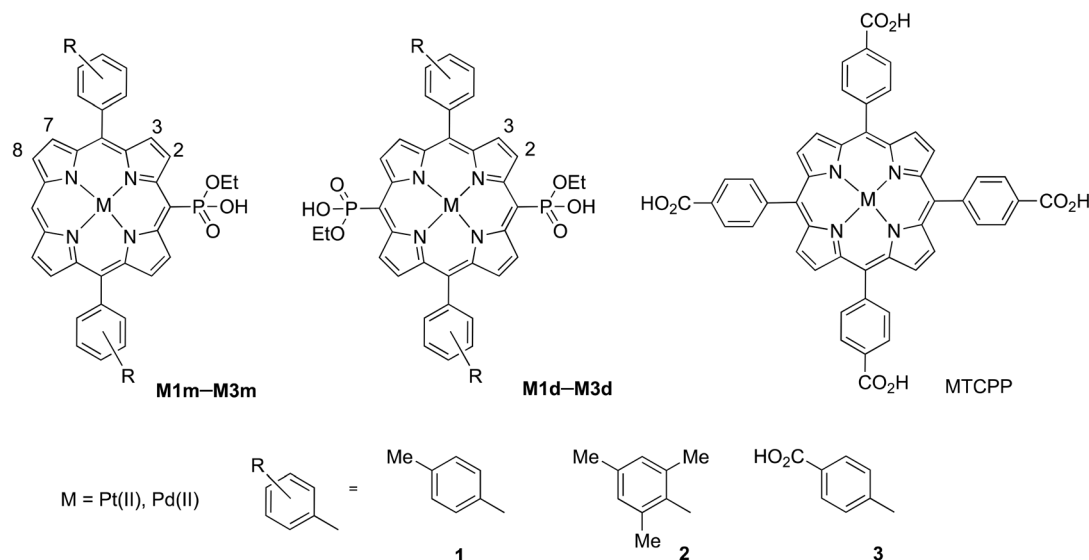
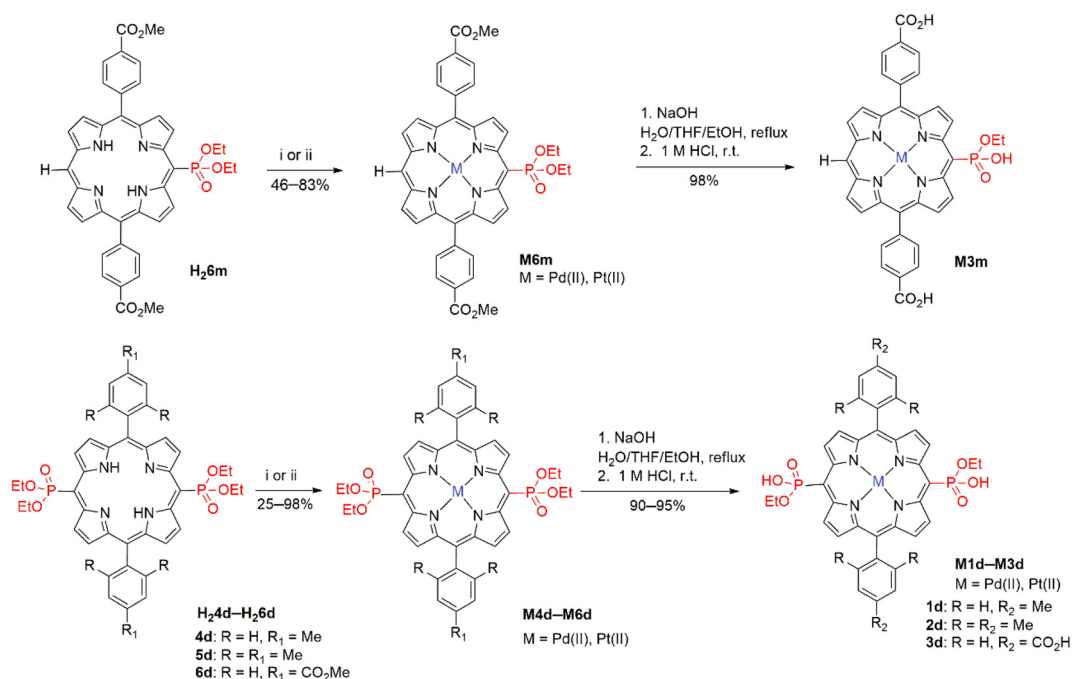


Fig. 1 Structures of porphyrins **M3m** and **M1d–M3d** studied in this work and of the reference compounds **M1m**, **M2m**, and **MTCPP**.



Scheme 1 Synthesis of phosphonate esters **M3m** and **M1d–M3d**. General conditions and reagents: (i) Pd(OAc)<sub>2</sub>, CHCl<sub>3</sub>/MeCN, reflux; (ii) PtCl<sub>2</sub>, PhCN, reflux, Ar.

us.<sup>61</sup> All palladium complexes **Pd6m** and **Pd4d–Pd6d** were obtained in high yields (>90%). In contrast, the synthesis of platinum complexes was more challenging, resulting in product yields of 25–57% after chromatographic purification, likely due to the partial decomposition of the porphyrins in boiling benzonitrile.

The hydrolysis of all complexes was carried out using sodium hydroxide in a boiling THF/EtOH/H<sub>2</sub>O (2 : 1 : 1 v/v/v) mixture. Notably, ethanol is more appropriate than methanol

to conduct this reaction, as performing the reaction in methanol could lead to partial transesterification of the ethyl phosphonate group, affording an inseparable mixture of products. The reaction course was monitored by MALDI-TOF spectrometry, and heating was stopped immediately after the consumption of the starting compounds. Pure (>90%) complexes **M3m** and **M1d–M3d** were isolated by filtration after acidification of the reaction mixtures to a pH below 2.5 with 0.5 M HCl. In the case of methoxycarbonyl-substituted porphyrins **M6m**

and **M6d**, both the carboxylate ester and the phosphonate diester groups were hydrolyzed under these conditions, yielding three- and tetraanionic complexes **M3m** and **M3d** which were isolated in near-quantitative yields.

The structures of the synthesized phosphonate esters **M4d-M6d**, **M3m** and **M1d-M3d** were confirmed by  $^1\text{H}$ ,  $^{13}\text{C}$ , and  $^{31}\text{P}$  NMR, FT-IR, and HRMS analyses (Fig. S39–S88†). In particular, for the target monoesters **M3m** and **M1d-M3d**, a characteristic upfield shift of the phosphorus signal by 3 ppm was observed compared to the diesters **M6m** and **M4d-M6d**. This signal was pH-dependent, shifting further upfield by 4 ppm upon the addition of 1  $\mu\text{L}$  of ammonia (25%) to the NMR tube.

### Solid-state structures of **M6d**

The diethyl phosphonates **Pd6d** and **Pt6d** were further characterized by single-crystal X-ray diffraction. Single crystals were grown by slow diffusion of *n*-hexane into a chloroform solution of these compounds. The complexes are isostructural and crystallize in the orthorhombic  $Pca2_1$  space group, with the asymmetric unit consisting of a single molecule (Fig. 2). A summary of the crystallographic data is provided in Table S1† and selected bond lengths and angles are presented in Tables S2–S5.† In these complexes, metal centers exhibit a square-planar coordination geometry formed by four pyrrole nitrogen atoms, with average M–N distances of 2.014(2) Å and 2.021(2) Å for **Pt6d** and **Pd6d**, respectively. These distances are consistent with those found in other Pt(II) and Pd(II) porphyrins.<sup>61–65</sup> The displacements of platinum and palladium atoms from the porphyrin mean plane are as small as 0.005 and 0.003 Å for **Pt6d** and **Pd6d**, respectively. The porphyrin macrocycle is almost flat, as the deviation of carbon atoms from the mean porphyrin plane of all 24 atoms does not exceed the values found for C(19) (*meso*-C atoms bearing the phosphoryl substituent) of

–0.148 and –0.152 Å for Pt(II) and Pd(II) complexes, respectively.

Both phosphoryl groups of the porphyrin point in the same direction with respect to the oxygen atoms. However, only one group lies nearly in the mean plane of the porphyrin, forming an intramolecular  $\text{C}_\beta\text{--H}\cdots\text{O}$  hydrogen bond, while the other group is slightly twisted, resulting in a larger distance to the hydrogen  $\text{C}_\beta\text{--H}$  and a smaller  $\text{C}_\beta\text{--H}\cdots\text{O}$  angle. The P–O bond distances of 1.454(2)–1.468(2) Å (for P=O) and 1.558(4)–1.590(4) Å (for P–O) are typical for diethoxyphosphoryl-substituted porphyrins.<sup>44,46</sup> The *meso*-phenyl substituents exhibit different twist angles (70.5 and 83.5° for **Pt6d**, 70.7 and 83.6° for **Pd6d**) with respect to the  $\text{N}_4$  plane. This difference is attributed to variations of the weak intermolecular interactions in which these substituents are involved in the crystals (Fig. S1†).

In the crystal, the molecules form a slipped columnar structure along the [010] direction, and these columns are arranged in zig-zag chains in the *ab* plane as shown in Fig. 3, S1 and S2† for **Pt6d**. Interestingly, the  $\pi$ – $\pi$  interactions between molecules in the column are weak. The distance between the porphyrin planes is 4.227 Å and tetrapyrrolic macrocycles are significantly shifted relative to each other, forming an angle of 54° between the centroid–centroid line and the normal to the planes. Most of the C $\cdots$ C and C $\cdots$ N distances between adjacent tetrapyrrolic macrocycles exceed 4.2 Å, short contacts being mainly observed between the hydrogen atoms of phenyl rings and the metal centers of adjacent molecules (Fig. 3 and Table S6†).

Such M $\cdots$ H interactions have been previously reported in Pt(II) and Pd(II) complexes. Pd/Pt $\cdots$ H hydrogen bonding distances of 2.2–2.5 Å have been observed in complexes with ligands bearing acidic hydrogens,<sup>66–69</sup> while much longer Pd/Pt $\cdots$ H distances (3.5–4.0 Å) are typical for ligands containing only C–H bonds available for coordination to metal centers.<sup>65,70</sup> Like other weak interactions, these contacts stabil-

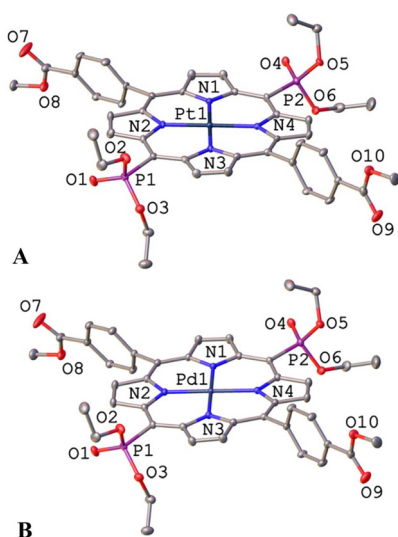


**Fig. 2** The asymmetric unit and respective view along the porphyrin plane of **Pt6d** (A) and **Pd6d** (B). Thermal ellipsoids are drawn at the 50% probability level.

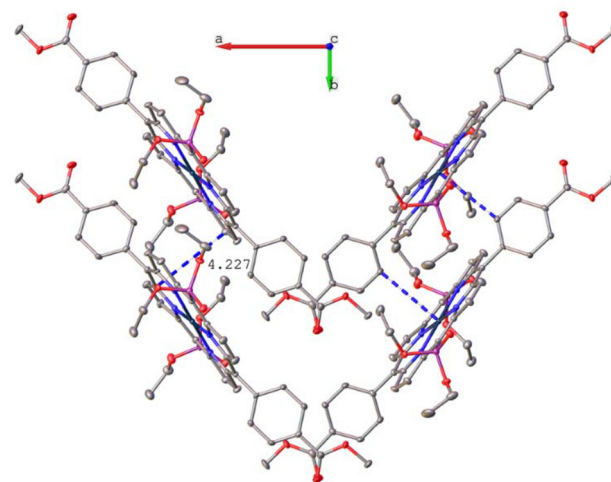


**Fig. 3** The crystal packing of two zig-zag chains of **Pt6d** along [001]. All hydrogen atoms have been omitted for clarity.



ize the lattice and may even influence ligand conformations in the crystal.<sup>70</sup>

Interestingly, the crystal packing observed for **Pd6d** and **Pt6d** is different from that of the less sterically hindered diesters **Pd6m** and **Pt6m** bearing a single phosphonate substituent at the tetrapyrrolic macrocycle.<sup>61</sup> In the crystal of these compounds, the phosphonate groups of adjacent molecules have opposite orientations which facilitates strong  $\pi$ - $\pi$  stacking of the aromatic macrocycles. This difference highlights the importance of the second phosphonate group attached to the porphyrin core on the structural organization of supramolecular assemblies and supports the hypothesis that this substituent could play a crucial role in the solution aggregation of these complexes.

### Investigation of solution aggregation by $^1\text{H}$ NMR spectroscopy

The aggregation of **Pt3m** and **Pd3m** in basic aqueous media was investigated by variable temperature (VT)  $^1\text{H}$  NMR spectroscopy in a temperature range spanning 303–363 K. The  $^1\text{H}$  NMR spectra of a  $1.5 \times 10^{-3}$  M solution of the complexes in  $\text{D}_2\text{O}$  (pD  $\sim$  12) are presented in Fig. 4 and S3–S7.†

As shown in Fig. 4, only four sets of signals are observed at 303 K, two partially resolved doublets and two broadened featureless signals. As the temperature gradually increases to 353 K, three additional signals from  $\text{H}_{\text{meso}}$ ,  $\text{H}_{\beta 7}$ , and  $\text{H}_{\beta 8}$  are observed. Further heating to 363 K is accompanied by coalescence of the  $\text{H}_{\beta 7}$  and  $\text{H}_{\beta 8}$  signals. The COSY NMR spectrum at 348 K shows cross-peaks between pairs of narrow signals, which enables the unambiguous assignment of four of the eight pyrrole moieties and all phenyl protons (Fig. S4†). We attributed the pyrrole protons already observed at 303 K to the rings oriented toward the phosphonate substituents ( $\text{H}_{\beta 2,3}$ ) due to the significant downfield shift of one doublet. The remaining pyrrole protons  $\text{H}_{\beta 7,8}$  and the  $\text{H}_{\text{meso}}$  proton do not show resolved peaks, probably because of the aggregation of molecules in the studied solution. The considerable upfield shift ( $>0.5$  ppm) and changes in signal line shapes of the

$\text{H}_{\text{meso}}$  and the  $\text{H}_{\beta 7,8}$  protons located in the *meso*-unsubstituted part of the porphyrin ring at room temperature indicate that these protons are more strongly affected by the ring-current effect of the  $\pi$  system of adjacent porphyrin compared to the other protons of the macrocycle. Such spectral behavior suggests that J-aggregates with an offset arrangement of macrocycles predominate in the studied solution, which agrees well with the arrangement observed in the crystal structure of corresponding bis-phosphonate diesters **M6d**. Similar spectral signatures of self-assembly in aqueous media were reported previously for analogous gallium(III) and indium(III) porphyrinates (**In3m** and **Ga3m**).<sup>47</sup> However, in contrast to In(III) and Ga(III) complexes, heating to 363 K was insufficient to obtain an entirely resolved spectrum of the monomer species.

It is known that addition of alcohol decreases the aggregation of porphyrins in water ( $\text{H}_2\text{O}$ ).<sup>71,72</sup> Therefore, we recorded  $^1\text{H}$  NMR spectra of **Pt3m** at 303 K in  $\text{D}_2\text{O}/\text{CD}_3\text{OD}$  mixtures of various compositions (Fig. S5†). Indeed, the  $^1\text{H}$  NMR spectrum of the complex in neat  $\text{CD}_3\text{OD}$  was well resolved and the spectral pattern corresponded to the target structure. 2D NOESY NMR experiments (Fig. S6†) allowed all the signals of **Pt3m** to be assigned. The signals of the  $\text{H}_{\text{meso}}$  and  $\text{H}_{\beta 7,8}$  pyrrole protons located in the unsubstituted part of the porphyrin experienced the largest shifts upon changing the  $\text{D}_2\text{O}:\text{CD}_3\text{OD}$  ratio from 0:100 to 100:0 v/v. This confirmed the involvement of these protons in the self-assembly process. Similar results were obtained for the corresponding Pd(II) complex **Pd3m**, which was investigated over the 278–363 K temperature range (Fig. 4 and S7†).

The  $^1\text{H}$  NMR spectra of the phosphonate-disubstituted complex **M3d** in  $\text{D}_2\text{O}$  (pD  $\sim$  12) at various temperatures are shown in Fig. 5, S8 and S9.† In this case, no significant ( $>0.1$  ppm) temperature-induced shifts of the signals were observed over the entire temperature range studied (273–363 K), and the spectra displayed well-resolved patterns of the target compounds above 313 K. At lower temperatures (273–313 K), all signals were slightly broadened and showed more pronounced upfield shifts compared to those appearing

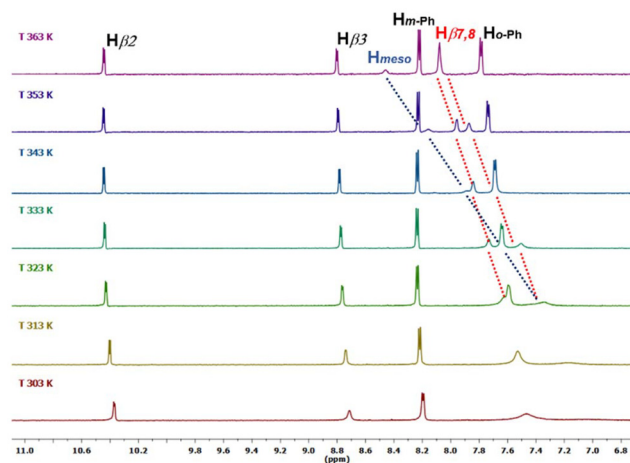


Fig. 4 Aromatic region of VT  $^1\text{H}$  NMR spectra of **Pd3m** in  $\text{D}_2\text{O}$ .  $C = 1.5 \times 10^{-3}$  M, pD  $\sim$  12. Proton labeling is presented in Fig. 1.

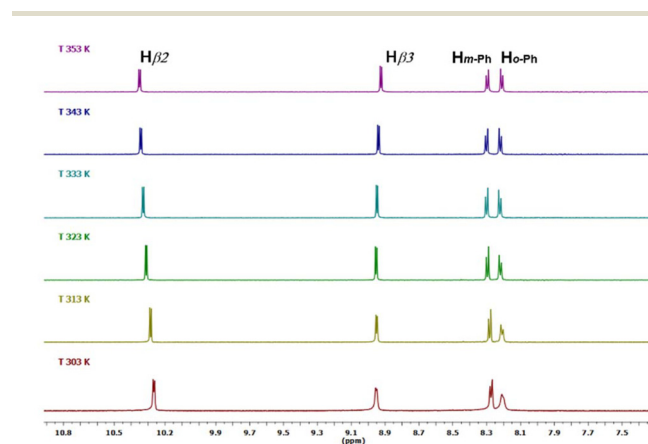


Fig. 5 Aromatic region of VT  $^1\text{H}$  NMR spectra of **Pd3d** in  $\text{D}_2\text{O}$ .  $C = 1.5 \times 10^{-3}$  M, pD  $\sim$  12. Proton labeling is presented in Fig. 1.

in the higher temperature region, particularly the phenyl *ortho*-H and the pyrrole protons adjacent to the phosphonate substituent. This behavior is likely due to a slowdown in the rotation rate of the anisotropic phenyl and phosphonate groups as the temperature decreases. Based on these data, we concluded that only the monomeric species exist in solution at room temperature and that they are predominant across the entire temperature range, although the aggregation of complex **M3d** in  $10^{-3}$  M aqueous media at low temperatures cannot be completely ruled out.

### Optical properties and photophysics

The electronic absorption spectra of **M3m** and **M1d–M3d** were recorded at 298 K in a buffered MOPS/DMF (9 : 1 v/v) mixture and in methanol (MeOH) basified with aqueous ammonia (25%; 1 drop). The data obtained in these studies are listed in Table 1, along with those of related water-soluble porphyrins reported previously.

All studied phosphonate-substituted complexes exhibit absorption profiles which are similar to those of their non-phosphonated analogues. In short, the spectra display an intense Soret band and two Q bands, with the absorption maxima of the Pt(II) complexes **Pt3m** and **Pt1d–Pt3d** being blue shifted by 4–14 nm compared to those of the analogous Pd(II) porphyrins **Pd3m** and **Pd1d–Pd3d**, respectively (Table 1, Fig. 6). The introduction of a second electron-withdrawing phosphonate group into the **M3m** molecules results in batho-

chromic shifts (5–26 nm) of all absorption maxima for both the Pt(II) and Pd(II) complexes investigated in this work.

Comparative studies of aggregation in the concentration range of  $10^{-6}$ – $10^{-4}$  M were conducted for complexes **Pt3m** and **Pt3d** in MOPS buffer (Fig. S19 and S20†). The strong aggregation of complex **Pt3m** in the studied solutions was ascertained by deviations from the Beer–Lambert law and bathochromic shifts of all absorption bands with increasing concentration, which are typical signatures for the formation of J-aggregates. These aggregates were also observed in more concentrated solutions ( $10^{-3}$  M, pH ~ 12) by NMR spectroscopy, as discussed above.

The aggregation of **Pt3m** was also studied by UV–vis spectrophotometry. In this case, the ionic strength ( $\mu_{\text{eff}}$ ) of the solutions was gradually increased by addition of sodium chloride (Fig. S20†). Under such conditions, the Soret and Q bands progressively shifted to high and low energy, respectively, suggesting that the molecular organization of the aggregates depends on the environment and is differently influenced by parameters such as concentration and  $\mu_{\text{eff}}$ . Notably, the isosbestic points in the spectra of solutions with  $\mu_{\text{eff}}$  ranging from 0.01 to 0.11 mol L<sup>-1</sup> suggest that probably only monomeric and dimeric species exist in these solutions.<sup>77,78</sup>

The spectroscopic behavior of the bis-phosphonate derivatives **M3d** was different, no deviation from the Beer–Lambert law was observed in the concentration range of  $10^{-6}$ – $10^{-4}$  M (Fig. S21†) and the spectra remained virtually superimposable when  $\mu_{\text{eff}}$  was gradually increased up to 0.81 mol L<sup>-1</sup> (Fig. S22†). Notably, *meso*-tetraarylporphyrins with the

**Table 1** Photophysical properties of the water-soluble complexes **M3m** and **M1d–M3d** and reference compounds<sup>a</sup>

Compound	Solvent	Absorption	Phosphorescence			Ref.
		$\lambda_{\text{abs}}$ (nm) ( $\epsilon \times 10^{-3}$ (M <sup>-1</sup> cm <sup>-1</sup> ))	$\lambda_{\text{em}}$ (nm)	$\Phi_{\text{em}}$ <sup>b</sup> (%)	$\tau$ (μs)	
<b>Pt3m</b>	MeOH <sup>c</sup>	395 (107), 510 (11), 542 (10)				This work
	Buffered H <sub>2</sub> O <sup>d</sup>		667, 731 (sh)	4.2	36	This work
<b>Pd3m</b>	MeOH <sup>c</sup>	407 (151), 522 (18), 553 (12)				This work
	Buffered H <sub>2</sub> O <sup>d</sup>		695, 762 (sh)	0.9	248	This work
<b>Pt1d</b>	Buffered H <sub>2</sub> O/DMF <sup>e</sup>	408 (129), 529 (12), 565 (9)				This work
<b>Pd1d</b>	Buffered H <sub>2</sub> O/DMF <sup>e</sup>	415 (132), 533 (8), 571 (10)				This work
<b>Pt2d</b>	Buffered H <sub>2</sub> O/DMF <sup>e</sup>	401 (153), 521 (9), 558 (14)				This work
<b>Pd2d</b>	Buffered H <sub>2</sub> O/DMF <sup>e</sup>	413 (148), 531 (7), 569 (12)				This work
<b>Pt3d</b>	MeOH <sup>c</sup>	400 (87), 525 (7), 560 (25)				This work
	Buffered H <sub>2</sub> O/DMF <sup>e</sup>	402 (182), 522 (11), 560 (15)				This work
	Buffered H <sub>2</sub> O <sup>d</sup>		720	1.4	22	This work
<b>Pd3d</b>	MeOH <sup>c</sup>	414 (174), 532 (10), 568 (10)				This work
	Buffered H <sub>2</sub> O/DMF <sup>e</sup>	413 (148), 531 (9), 569 (12)				This work
	Buffered H <sub>2</sub> O <sup>d</sup>		746	0.4	175	This work
PtTCPP	Buffered H <sub>2</sub> O/DMF <sup>e</sup>	401 (172), 509 (16)				This work
	H <sub>2</sub> O/ethylene glycol (9 : 1)	403 (184), 510 (17), 539 (4)	651	1.7	50	73
PdTCPP	Buffered H <sub>2</sub> O <sup>f</sup>	413 (270), 523 (21), 554 (sh)	701	0.9	300	73
PdTSPP <sup>g</sup>	H <sub>2</sub> O	412 (127), 520 (11)	695, 760	0.7	350	74
PdTSBP <sup>g</sup>	H <sub>2</sub> O <sup>h</sup>		790	2.3	310	75
PtTSPP <sup>i</sup>	H <sub>2</sub> O/ethylene glycol (9 : 1)	402 (133), 510 (14), 540 (6)	645	1.3	60	76
PtTMPyP	H <sub>2</sub> O <sup>j</sup>	401 (164), 513 (17), 545 (11)	651	0.3	2.3	76

<sup>a</sup> In deoxygenated (by N<sub>2</sub> bubbling for 15 min) solutions at  $C = 1 \times 10^{-6}$  M. Additional data are presented in Fig. S10–18 and S21.† <sup>b</sup> The absolute emission quantum yields were determined with an integrating sphere. <sup>c</sup> One drop of aqueous ammonia (25%) was added in the cuvette.  $T = 298$  K. <sup>d</sup> Buffered water, [MOPS] = 0.01 M, pH = 7.2,  $C = 1 \times 10^{-6}$  M (for UV–vis studies). <sup>e</sup> Buffered water/DMF (9 : 1 v/v) mixture, [MOPS] = 0.05 M, pH = 7.2,  $\mu_{\text{eff}} = 0.1$  mol L<sup>-1</sup>, [NaCl] = 0.075 M,  $T = 298$  K. <sup>f</sup> Aqueous solution,  $\mu_{\text{eff}} = 0.1$  mol L<sup>-1</sup> (NaOH),  $C = 1 \times 10^{-6}$  M (for UV–vis studies). <sup>g</sup> PdTSBP = Pd(II) complex of sulphonated tetrabenzoporphyrin. For structure see ref. 75. <sup>h</sup> Aqueous solutions deoxygenated with the glucose oxidase–catalase system, room temperature (RT). <sup>i</sup> H<sub>2</sub>TSPP = *meso*-tetra(*p*-sulfonatophenyl)porphyrin. <sup>j</sup>  $T = 298$  K.

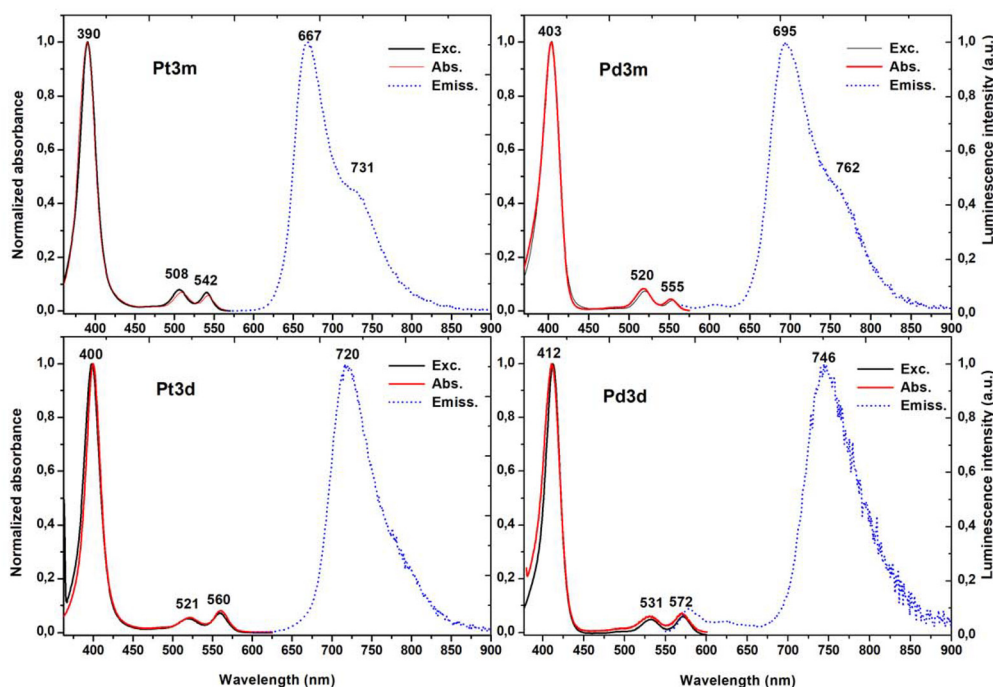


**Fig. 6** Excitation [ $\lambda_{\text{em}} = \lambda_{\text{max}}(\text{phosp.})$  (nm)], UV-vis absorption and emission [ $\lambda_{\text{ex}} = \lambda_{\text{abs}} Q(1,0)$  (nm)] spectra of **M3m** and **M3d** in 0.01 M MOPS buffer pH 7.2,  $C = 1 \times 10^{-5}$  M for Pt(II) complexes or  $C = 5 \times 10^{-6}$  M for Pd(II) complexes.

*p*-carboxy- and *p*-sulfonato-substituted phenyl ring (PdTCPP and PdTSPP) form aggregates under the same conditions, while only the positively charged Pt/Pd tetrakis(*N*-methyl-4-pyridinium)porphyrins (PtTMPyP and PdTMPyP) stay monomeric in pure water up to  $1 \times 10^{-3}$  M.<sup>76,79</sup>

Next, we compared the aggregation of **Pt3d** and PtTCPP at different pH values. Below pH  $\sim 4$ , the absorption spectra of freshly prepared  $5.4 \times 10^{-6}$  M aqueous solutions of **Pt3d** containing 0.1 M NaCl were found to change over time, the spectral modifications monitored over 3 h being the most pronounced at the lowest examined pH value of 2.5 (Fig. S23†). For the three solutions at pH 4.0, 3.5, and 3.0, the intensity of the Soret and Q bands gradually decreased, while the latter also underwent a bathochromic shift, whereas the baseline drift at wavelengths higher than 600 nm clearly pointed out light diffusion and thus the progressive appearance of particles. At pH 2.5, all these phenomena were amplified, but moreover the Soret band broadened and shifted to lower energy, while the intensity of the low-energy Q band increased in this case. Progressive protonation of the *p*-carboxyphenyl groups below pH 4 lowers the overall charge and thus the water solubility of the protonated species that tend to slowly aggregate and ultimately precipitate. Hence, a spectrophotometric titration of the soluble tetraanionic **Pt3d** complex with hydrochloric acid was undertaken from pH 10.65 down to pH 3.57 (Fig. S25†). The absorption spectra were recorded immediately after the addition of the acid aliquots to limit the slow aggregation process occurring below pH 4. The intensity decreases of both the Soret and Q bands together with a concomitant red shift of the latter become significant below pH 5.

The isosbestic points at 420, 502, and 541 nm further suggested the formation of a singly protonated porphyrin. Multiwavelength data analysis of the entire dataset ( $350 \leq \lambda \leq 650$  nm; 30 spectra from pH 10.65 to 3.57) using the HypSpec software returned a protonation constant of  $\log K \sim 3.6$ . This value has to be taken as approximate, as the spectra between pH 4 and 3.5 might already be slightly off equilibrium, while the protonated fraction reaches only about 50% at the lowest considered pH value. The calculated absorption spectra for  $[\text{Pt3d}]^{4-}$  and  $[\text{Pt3dH}]^{3-}$ , the distribution diagram and calculated vs. experimental optical densities at 400 nm are displayed in Fig. S26–28.† Attempts to fit the data with other chemical models ( $[\text{Pt3d}]^{4-}$  and  $[\text{Pt3dH}_2]^{2-}$ , or  $[\text{Pt3d}]^{4-}$ ,  $[\text{Pt3dH}]^{3-}$ , and  $[\text{Pt3dH}_2]^{2-}$ ) failed as unrealistic electronic spectra were computed for some species. Considering the electron withdrawing effect of the metalloporphyrin ring, the refined  $\log K$  value of 3.6 is in rather good agreement with the protonation constant reported for benzoate ( $\log K = 4.01$  at  $\mu_{\text{eff}} = 0.1$  mol L $^{-1}$ ,  $T = 298.2$  K) or 4-allylbenzoate ( $\log K = 4.34$  at  $\mu_{\text{eff}} = 0$  mol L $^{-1}$  or  $\log K = 4.1$  if the value at infinite dilution is extrapolated to  $\mu_{\text{eff}} = 0.1$  mol L $^{-1}$  using the Davies equation,  $T = 298.2$  K).<sup>80</sup>

In the case of PtTCPP, broadening of the Soret band and a light-scattering-induced increase of the baseline level were observed in the pH range 3.55–6.37, indicating a high degree of porphyrin aggregation in mild acidic solutions. A well-resolved, pH independent UV-vis absorption spectrum could only be recorded under basic conditions (pH  $> 8$ ), where the porphyrin exists predominantly as a tetra-anionic species.

Thus, replacement of two *p*-carboxyphenyl groups of MTCPP by the more acidic and bulky ethyl phosphonate sub-

stituents significantly decreases the degree of porphyrin aggregation in aqueous media and enables the concentration, pH, and ionic strength ranges in which porphyrins exist as monomeric species to be widened.

As expected, complexes **M3m** and **M3d** are phosphorescent in deoxygenated aqueous solutions (0.01 M MOPS buffer, pH 7.2, RT, Fig. 6). The excitation and ground-state absorption spectra of all the studied compounds are very similar. The maxima of phosphorescence of the Pt(II) complex are shifted to the lower energy regions in comparison with those of the Pd(II) complexes, similar to what was observed for the absorption spectra (Fig. 6 and Table 1). A bathochromic shift of the main emission band by *ca.* 50 nm and the disappearance of the low energy shoulder typical of only A<sub>2</sub>B-type porphyrins are observed in the spectra of the bis-phosphonates **M3d**. No fluorescence is detectable for the Pt(II) complexes and very little fluorescence ( $\Phi_f < 0.1\%$ ),  $\tau = 3.75$  ns, for the respective Pd(II) derivatives. Excitation spectra (Fig. S24B†) that were acquired for the fluorescence and phosphorescence bands show the same spectral features as the absorption spectrum (Fig. S24C†) which confirms that the fluorescence indeed originates from the Pd(II) complex and not from an impurity.

The absolute quantum yields ( $\Phi_{em}$ ) and luminescence lifetimes ( $\tau$ ) of **M3m** measured in deaerated MOPS buffer were 2–6.5 times lower (4.2% and 36  $\mu$ s for **Pt3m**, 0.9% and 248  $\mu$ s for **Pd3m**) compared to the values for dialkyl phosphonates **M6m** in toluene<sup>61</sup> due to water quenching effects.<sup>81</sup> The addition of a second phosphonate group at the *meso*-position of the luminophore molecule decreases  $\Phi_{em}$  by more than 2-fold, and  $\tau$  decreases by about 1.5-fold. This reduction of both  $\Phi_{em}$  and  $\tau$  likely reflects the increased probability of non-radiative deactivation processes of the triplet excited state. A similar effect was observed previously for dialkyl phosphonates in toluene.<sup>61</sup>

Aggregation of **M3m** at high ionic strength values (0.41 M) is accompanied by a decrease in  $\Phi_{em}$  (Fig. S22†), similarly to Pt(II) and Pd(II) complexes with the H<sub>2</sub>TCPP ligand.<sup>73</sup> In contrast, for the **M3d** complexes, the intensity of emission was not influenced by ionic strength changes under the same solution conditions, in agreement with the absence of aggregation observed by UV-vis studies.

Comparison of the photophysical properties of the water-soluble complexes reported in this work with those of well-known complexes that have been extensively used in biological experiments (Table 1) enables to conclude that the phosphorylated metalloporphyrins described herein may act as effective PSs for biological applications. Indeed, their photophysical characteristics are comparable to those of other negatively and positively charged water-soluble Pd(II) and Pt(II) complexes. To further validate this, we examined the energy transfer efficiency from the triplet state of **M3d** to molecular oxygen, resulting in the production of singlet oxygen.

The efficiency of oxygen quenching was investigated by the Stern–Volmer method only for the non-aggregating disubstituted phosphorylated porphyrin **Pt3d**, because the Pd(II) complex shows low luminescence brightness and a very high

sensitivity even at low dioxygen partial pressure ( $pO_2$ ) in solution, making quantitative measurements challenging. A linear dependency of  $\tau_0/\tau$  on  $pO_2$  in 0.02 M MOPS buffer was observed and the data were treated using the Stern–Volmer equation (Fig. 7). The calculated  $K_{SV}$  value for **Pt3d** was 0.045 hPa<sup>−1</sup> ( $3.66 \times 10^4$  M<sup>−1</sup>), which is comparable to that reported for the water-soluble cationic PtTMPyP ( $K_{SV} = 2.2 \times 10^4$  M<sup>−1</sup>)<sup>82</sup> and anionic PtTCPP ( $K_{SV} = 7.2 \times 10^4$  M<sup>−1</sup>)<sup>83</sup> porphyrins.

To evaluate the photosensitizing efficiency of **Pd3d**, the quantum yield of singlet oxygen generation was determined by means of the spin-trapping EPR technique. This method is based on comparing the rate of radical production during the reaction of a singlet-oxygen trap, irradiated in aerated solutions containing the target and a reference PS. The EPR approach is particularly advantageous as it enables measurements across a wide range of solvents and even under *operando* conditions by irradiating samples directly within the EPR spectrometer cavity. However, EPR remains underutilized for quantitative measurements due to instrumental limitations and the potential contribution of side electron-transfer processes involving the singlet-oxygen trap, which can also lead to the formation of observed radicals.<sup>55,84</sup> For our measurements in pure water, we used 4-oxotetramethylpiperidine (4-oxo-TEMP) as the singlet-oxygen trap, which has never been used so far for quantitative measurements to the best of our knowledge. In a first attempt, the classical phenalenone was employed as a reference compound. The buildup of the characteristic 4-oxo-TEMP radical signal was monitored over time, while irradiating with a 365 nm LED the aqueous solutions of this PS and isoabsorbing solutions of PdTCPP or **Pd3d**. At the selected wavelength, where only a residual absorbance of the porphyrin Soret band is observed, unrealistically high values of singlet oxygen quantum yields ( $\Phi_\Delta$ ) were obtained for the porphyrins. Thus, in a subsequent series of experiments, we switched to Rose Bengal as the reference compound and used a green LED (530 nm) for irradiation, as the latter wavelength matches well with the porphyrin Q band. Under these revised conditions, all three studied PSs exhibited similar efficiencies in generating singlet oxygen (Fig. S29†), with  $\Phi_\Delta$  values of 0.80 and 0.78 for PdTCPP and **Pd3d**, respectively, assuming  $\Phi_\Delta = 0.75$  for Rose Bengal.<sup>85</sup> These values are in good agreement

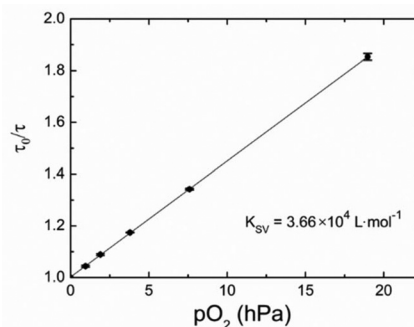


Fig. 7 Stern–Volmer plot for **Pt3d** in aqueous media. [MOPS] = 0.02 M, pH 7.2, [NaCl] = 0.1 M,  $T = 298$  K.



with those previously reported for PdTCPP in an aqueous solution (0.7) with  $\mu_{\text{eff}} = 0.15 \text{ mol L}^{-1}$  ( $\text{NaNO}_3$ ), considering that an increase in ionic strength generally leads to a decrease in  $\Phi_{\Delta}$  in aqueous solutions.<sup>86</sup>

Thus, the  $\Phi_{\Delta}$  value obtained for **Pd3d** is comparable to those reported for porphyrins of interest like those used in PDT.<sup>50,84,87,88</sup> These results underscore the high potential of the metalloporphyrins evaluated herein as water-soluble phosphorescent oxygen probes and PSs for PDT, as well as for aqueous photocatalytic oxidation reactions for which molecular oxygen is used as a terminal oxidant.

### Photostability studies

The photostability of oxygen-sensing probes and PSs is a key point for practical applications. Although photostability is strongly influenced by environmental factors, preliminary insights into photobleaching are useful. The photobleaching of porphyrins should be studied over extended time periods because it rarely follows first-order kinetics and often significantly accelerates over time, owing to radical formation.<sup>61</sup> One general strategy to reduce photooxidation caused by photosensitized singlet oxygen and other reactive oxygen species is the incorporation of electron-withdrawing groups into the lumiphore structure.<sup>53,89–91</sup> Therefore, we expected that the introduction of electron-withdrawing phosphonate groups may help slow down these unfavorable reactions.

The photodegradation study of complexes **M1d–M3d** was conducted in a  $\text{H}_2\text{O}/\text{DMF}$  mixture (9 : 1 v/v), where the complexes showed no spectroscopic signs of aggregation in the  $10^{-6}$ – $10^{-4}$  M concentration range. Solutions of the porphyrins ( $5 \times 10^{-6}$  M) were irradiated using an Osram Powerstar HQI BT 400 W lamp (Fig. S37†), and their photobleaching was monitored by vis–NIR absorption spectrophotometry according to the procedure previously reported by us, which allows for semi-quantitative comparisons within a defined series of analogous chromophores.<sup>61</sup>

As shown in Fig. 8, the rate of porphyrin bleaching strongly depends on the metal centers, with Pt(II) complexes exhibiting

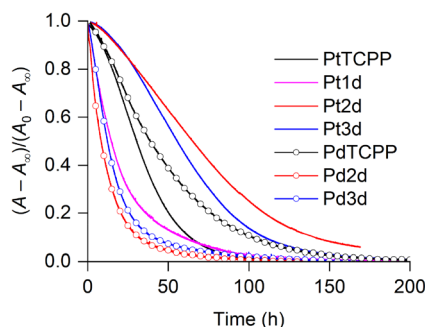


**Fig. 8** Photodegradation kinetics of Pt(II) (line) and Pd(II) (line with circles) porphyrins ( $C = 5 \times 10^{-6}$  M) in buffered  $\text{H}_2\text{O}/\text{DMF}$  (9 : 1 v/v) mixture under vis–NIR irradiation using an Osram Powerstat HQI BT 400 W lamp. The absorbance ( $A$ ) changes over time were monitored at the maximum of the Soret band.  $[\text{MOPS}] = 0.05 \text{ M}$ ,  $\text{pH} = 7.2$ ,  $\mu_{\text{eff}} = 0.1 \text{ mol L}^{-1}$ ,  $[\text{NaCl}] = 0.075 \text{ M}$ ,  $T = 298.2(5) \text{ K}$ ,  $l = 1 \text{ cm}$ .

in most case greater stability than their Pd(II) analogues. Furthermore, peripheral substituents influence the peculiar shape of the kinetic traces. Among the Pt(II) phosphonate-substituted complexes, only **Pt1d**, which bears tolyl groups at the macrocycle, degraded more rapidly than PtTCPP. Surprisingly, PdTCPP demonstrated the highest stability among the Pd(II) complexes studied in this work; however, the kinetic traces of all studied Pd(II) complexes were quite similar, particularly for PdTCPP and **Pd3d**, during the initial stages of photobleaching.

When Pd(II) complexes were studied under the irradiation conditions used hereafter for photocatalytic experiments (425 nm LED, 18 W) in a  $\text{MeCN}/\text{H}_2\text{O}$  (4 : 1 v/v) mixture, the photobleaching exhibited an inverse trend: **Pd2d** and **Pd3d** were significantly more stable than PdTCPP, as shown in Fig. S38.† Interestingly, **Pd3d** demonstrated greater photostability than mesityl-substituted **Pd2d**, despite the presence of *ortho*-hydrogen atoms in the aryl substituents of this compound. Overall, these results were encouraging for the practical use of metalloporphyrins synthesized herein, which prompted us to test them as photocatalysts in oxidation reactions.

### Photocatalytic properties in oxidation reactions

Porphyrin-based photosensitizers are of significant interest in organic synthesis, primarily because they allow the replacement of toxic and hazardous oxidants by molecular oxygen in oxidation reactions, which are among the most dangerous processes in the production of fine chemicals. Performing these photooxidation reactions with water-soluble PSs enhances process sustainability, as this enables the reactions to be carried out in green solvents, while the PSs can be recovered through extraction into an aqueous phase. Metalloporphyrins have already been used successfully in the oxidation of alkanes, alkenes, alcohols, aldehydes, and sulfides.<sup>92–94</sup> Sulfides, however, are particularly challenging substrates because sulfoxides can be easily overoxidized, yielding sulfones, and C–S bond cleavage reactions can proceed as side reactions, while only selective oxidation processes are desirable.<sup>95,96</sup> The oxidation of these compounds could proceed either through the generation of electrophilic singlet oxygen *via* the energy transfer (EnT) process (Scheme S1,† route A) or through electron transfer (ET) (Scheme S1,† routes B and C), making predictions about the photocatalyst behavior challenging.

Among the Pd(II) complexes prepared in this work, tetra-anionic **Pd3d** is particularly interesting due to its high solubility in aqueous media and its efficiency in generating singlet oxygen. Complex **Pd2d**, featuring two mesityl substituents, also stood out as a photocatalyst of practical interest within the studied series. Previous investigations have shown that porphyrins with perfluorinated or sterically hindered *ortho*-disubstituted aryl groups at the *meso*-positions of the macrocycle exhibit superior catalytic activity in oxidation reactions (so-called second-generation catalysts),<sup>92,97–99</sup> because of restricted intermolecular processes (such as  $\mu$ -oxo bridge formation) involved in the photodegradation of the catalyst.

The photocatalytic properties of **Pd3d** were investigated by oxidizing various sulfides in a MeCN/H<sub>2</sub>O mixture (4 : 1 v/v) under a pure oxygen atmosphere and irradiation with a 425 nm LED (18 W). As shown in Scheme 2, most of the aryl methyl sulfides were transformed to sulfoxides almost quantitatively, although with various reaction times, and less than 2% of sulfone overoxidation products were observed in these reactions.

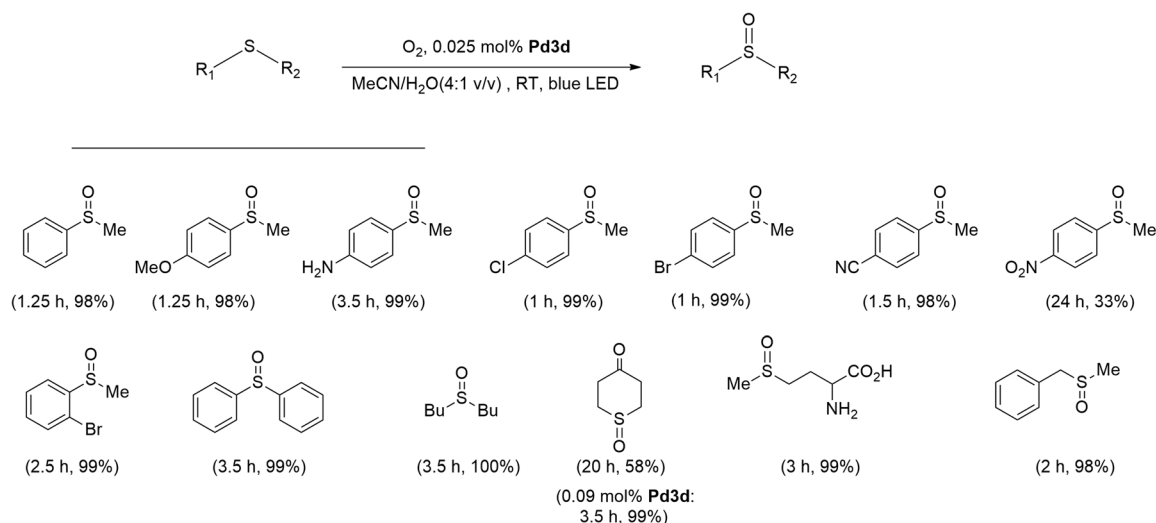
Electron-rich 4-methoxythioanisole and electron-deficient 4-halophenyl- or 4-cyanophenyl methyl sulfides exhibited high reactivity and their oxidation was complete in 1–1.5 h. Bulky *ortho*-bromothioanisole was oxidized in 2.5 h, which is only 2.5 times longer than the reaction time for *para*-bromo- and chloro-substituted analogues. 4-Aminophenyl methyl sulfide, which contains an amino group capable of participating in electro-transfer side reactions, also gave excellent results, although the time needed to reach complete conversion was longer (3.5 h) compared to that required for thioanisole oxidation. In contrast, 4-nitrothioanisole, known for its inertness in EnT reactions,<sup>100</sup> exhibited a significantly slower oxidation rate, with only 33% conversion after 24 h of irradiation. Dibutyl sulfide also reacted smoothly under these conditions, producing sulfoxide in almost quantitative yields within 3.5 h. Another dialkyl sulfide, cyclic thian-4-one, exhibited lower reactivity but was successfully oxygenated by increasing the photocatalyst loading to 0.09 mol%. Methionine sulfoxide, which has pharmaceutical applications, was obtained in nearly quantitative yield after 3 h of irradiation. Notably, high selectivity in oxidation was observed in the oxygenation of benzyl methyl sulfide, a substrate known to produce by-products due to undesired cleavage of the S–C bond during photocatalytic oxidation in acetonitrile.<sup>101</sup> Remarkably, diphenyl sulfide, known<sup>102</sup> for its resistance to photooxidation in the presence of PSs due to its low nucleophilicity and steric hindrance, was efficiently oxidized to sulfoxide in 3.5 h. Most of the sulfoxides thus obtained can be easily isolated in pure

form (>98%) without additional purification by column chromatography.

Once the oxidation reaction was complete, catalyst recycling was carried out by extracting **Pd3d** into an aqueous solution at pH 7–8. The photooxidation was performed in MeCN/H<sub>2</sub>O mixtures with a higher water content (1 : 1 v/v) to facilitate the phase separation and avoid the evaporation of the aqueous solution during the work-up process. Five consecutive oxidation reactions of 4-chloroanisole were conducted, yielding the target product almost quantitatively. However, full conversion in the final cycle required 4 h of irradiation, likely due to partial photodegradation of the catalyst during the reaction and some loss of catalyst in each work-up procedure.

Comparative studies of **Pd3d** and its mesityl analogue **Pd2d** were performed using diphenyl sulfide, 4-cyanophenyl, and 4-aminophenyl methyl sulfides. Diphenyl sulfide and 4-cyanophenyl methyl sulfide yielded sulfoxides in 3.5 h and 1.5 h, respectively, with both photocatalysts. The oxidation of the electron-rich 4-aminophenyl methyl sulfide proceeded more rapidly with **Pd3d**, taking only 3.5 h, but required 5 h with **Pd2d**. Additionally, extraction of **Pd2d** into an aqueous phase after completion of the reaction was only possible using 0.1 M aqueous sodium hydroxide. Consequently, this preliminary study revealed that **Pd3d** exhibited more advantageous catalytic features over **Pd2d** in photooxidation reactions, despite the presence of *ortho*-H on aryl residues of this compound.

Finally, the photocatalytic properties of **Pd3d** and PdTCPP were compared using the same series of aryl methyl sulfides (Table S7†). Both photocatalysts demonstrated comparable efficiency in the oxidation of most reactive sulfides; however, electron-poor sulfides systematically reacted more rapidly with **Pd3d**. For instance, the oxidation of 4-chlorophenyl methyl sulfide proceeded in 1 h with **Pd3d**, requiring 3.5 h of irradiation with PdTCPP. The irradiation time for diphenyl sulfide was reduced from 8 h to 3.5 h when PdTCPP was replaced by **Pd3d**.



**Scheme 2** Photocatalytic oxidation of sulfides by molecular oxygen using **Pd3d**.

Comparing the reactivity of different types of sulfides in the presence of **Pd3d** and PdTCPP, we hypothesized that the sulfoxidation reaction primarily proceeds through the EnT mechanism when PdTCPP is used as a photocatalyst. However, both the EnT and ET mechanisms may be involved when **Pd3d** is used (Scheme S1†).<sup>103–105</sup> To gain a deeper insight into the reaction pathway, the abilities of **Pd2d**, **Pd3d**, and PdTCPP to generate singlet oxygen in a MeCN/H<sub>2</sub>O mixture (4 : 1 v/v) were compared. This was a challenging issue to tackle, since no reference compound has been reported for this solvent mixture. We chose phenalenone (**PH**) as the reference, as its singlet oxygen quantum yield remains in the range of  $\Phi_{\Delta} = 0.95$ –1.00 regardless of the solvent, including pure MeCN and water. Since our EPR experiments with **PH** were dubious, as discussed above, we employed the fluorescence chemical trapping method using 1,9-anthracenedipropionic acid (ADPA). Upon irradiation at 395–405 nm of air-saturated solutions containing each complex, the compound selectively reacts with singlet oxygen, forming the corresponding endoperoxide. Monitoring the time course of luminescence decay upon prolonged irradiation gives indirect access to the quantum yield of singlet oxygen generation, as established in our previous work.<sup>106</sup>

In order to reinforce the validity of the measurements in MeCN/H<sub>2</sub>O, we used tris(bipyridyl)dichlororuthenium(II) as a model compound, which shares a similar range of excitation wavelengths, and for which the quantum yields of singlet oxygen generation in several solvents are available ( $\Phi_{\Delta} = 0.57$  in pure acetonitrile<sup>107</sup>). In this preliminary experiment, we demonstrated that the decrease in ADPA fluorescence, plotted as  $\ln(I_0/I)$  over time, is linear ( $R^2 < 0.995$ ) for both phenalenone and [Ru(bpy)<sub>3</sub>]Cl<sub>2</sub> (Fig. S31†) and yields  $\Phi_{\Delta} = 0.51$  considering  $\Phi_{\Delta} = 0.97$  for **PH**.

UV-vis studies of **Pd1d**–**Pd3d** in a MeCN/H<sub>2</sub>O mixture (4 : 1 v/v) at concentrations approximately 2–3 times lower than those used in photocatalytic experiments ( $A_{\max} < 0.25$ ) demonstrated that these complexes tend to aggregate in this solvent mixture (Fig. S30†). The broadening of the Soret band was most pronounced for **Pd1d**, but aggregate formation could not be entirely ruled out even for the most hydrophilic **Pd3d**.

This was evident as the spectrum of the solution prepared from a powdered sample obtained by ultrasonic treatment (trace **Pd3d**(1) in Fig. 9 and S30†) differed slightly from that of the diluted solution prepared from the aqueous stock solution (trace **Pd3d**(2) in Fig. 9 and S30†), the former showing less broadening of the Soret band as compared to the latter. Consequently, the  $\Phi_{\Delta}$  values measured for these two solutions of **Pd3d** were 0.88 and 0.76, respectively (Fig. S32 and S33†). **Pd1d** and **Pd2d** were also efficient in generating singlet oxygen, with  $\Phi_{\Delta}$  values of 0.77 and 0.76, respectively (Fig. S34 and S35†), which are both higher than that found for classical PdTCPP (0.58) in the same solvent (Fig. S36†).

Thus, the high efficiency of phosphonate-substituted porphyrins in the sulfide photooxidation can likely be attributed to their superior ability to generate singlet oxygen and high photostability in a MeCN/H<sub>2</sub>O mixture. However, both **Pd2d**

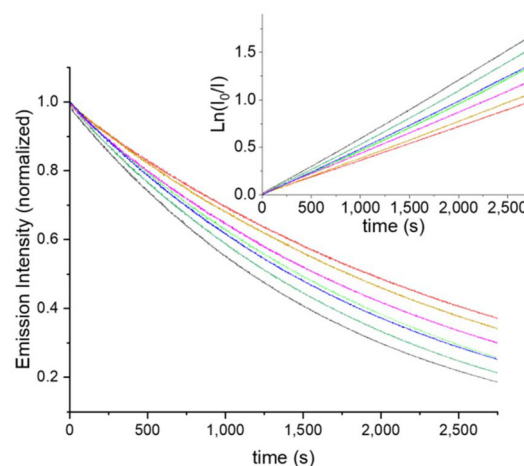


Fig. 9 Continuous monitoring of the decay in ADPA emission upon prolonged irradiation at 397–400 nm wavelength ( $P = 5$  mW (constant)) of isoabsorbing PS/ADPA mixtures in MeCN/H<sub>2</sub>O (4 : 1 v/v). Color code: phenalenone (black); [Ru(bpy)<sub>3</sub>]Cl<sub>2</sub> (red); **Pd1d** (blue); **Pd2d** (magenta); **Pd3d**(1) (dark green/olive); **Pd3d**(2) (light green); PdTCPP (yellow). Inset: first-order linear regressions ( $\ln(I_0/I)$  vs. time).

and **Pd3d** are efficient in the oxygenation of diphenyl sulfide, a compound known for its negligible reactivity with singlet oxygen. In this particular case, the main reaction pathway likely involves electron transfer. The triplet state of **Pd2d** and **Pd3d** may exhibit a higher oxidation potential than PdTCPP due to the electron-withdrawing nature of the phosphonate substituent. If so, these new phosphonate-substituted porphyrins could prove to be more effective photoredox catalysts than PdTCPP.

## Conclusions

A new type of water-soluble Pt/Pd porphyrins bearing one (**M3m**) or two ethoxyhydroxyphosphoryl substituents (**M1d**–**M3d**) directly attached to the tetrapyrrolic macrocycle has been synthesized by alkaline hydrolysis of the corresponding dialkyl phosphonate esters **M6m** and **M4d**–**M6d**. Complexes bearing different aryl substituents were obtained in high (palladium) or moderate (platinum) yields, demonstrating that this synthetic approach is general and enables the rational structural design of a series of compounds that are useful in oxidation photocatalysis.

The complexes thus obtained are quite soluble in basic aqueous media, although their aggregation propensity in solution depends on the number of phosphonate groups appended to the macrocycle. While mono-phosphonates **M3m** tend to form aggregates similarly to PdTCPP, the bulky bis-phosphonates **M3d** exist predominantly as monomeric species across a wide range of concentrations, ionic strengths, and pH values (4–12).

Structural studies of the diethyl phosphonate derivatives **Pt6d** and **Pd6d** demonstrated that the introduction of a second

phosphonate group indeed plays a decisive role in reducing the  $\pi$ - $\pi$  stacking of adjacent porphyrin molecules in the crystals. This reduction in stacking interactions likely contributes to the decrease in solution aggregation of **M3d**. Another important structural factor of these compounds is their lower molecular symmetry compared to typical water-soluble porphyrin derivatives bearing four identical *meso*-aryl substituents, such as aryl-4-carboxylates and aryl-4-sulfonates, which are structurally predisposed to form aggregates in aqueous media due to the formation of multiple electrostatic interactions.

We also demonstrated that the Pd/Pt porphyrins with phosphonate ester groups are phosphorescent in aqueous media, which is an important feature for biomedical or photocatalytic applications. Complexes **Pd1d–Pd3d** produce singlet oxygen with high efficiency in both MeCN/H<sub>2</sub>O mixtures and pure water. The platinum complex **Pt3d** turned out to be an efficient singlet oxygen sensitizer in buffered aqueous solution, comparable to previously reported cationic PtTMPyP<sup>4+</sup> and anionic PtTCPP complexes. Therefore, this new family of Pd/Pt porphyrins holds promises for a wide range of practical applications.

In this work, we demonstrated that **Pd3d** is a more efficient catalyst than PdTCPP for the selective photooxidation of sulfides to sulfoxides. This complex enables faster oxidation reactions under environmentally friendly conditions, utilizing dioxygen as the terminal oxidant and non-chlorinated solvents. Furthermore, this photocatalyst can be easily separated from the products and reused in consecutive catalytic cycles.

Beyond their use as photosensitizers and photoredox catalysts, these compounds are also of interest as precursors of functional materials, because both carboxylic and phosphonic groups are widely used in material chemistry, each serving as an anchor for specific inorganic supports. These compounds are also intriguing linkers for MOF synthesis, which could potentially increase the structural diversity of porous frameworks that have so far been primarily derived from PdTCPP in applied chemistry.

## Experimental

### Synthesis

General information on materials, methods, and synthesis of metalloporphyrins is provided in the ESI.†

### X-ray structural studies

Single crystals of **Pt6d** and **Pd6d** were obtained by slow diffusion of *n*-hexane into the solution of these complexes in chloroform. Crystals were mounted onto a glass needle using silicone oil, and cooled to the data collection temperature of 100 K. X-ray diffraction experiments for single crystals were performed on a Bruker Kappa Apex II automatic four-circle diffractometer equipped with an area detector (Mo-K $\alpha$  sealed-tube X-ray source,  $\lambda$  = 0.71073 Å, graphite monochromator). The unit cell parameters were refined over the whole dataset

using SAINT-Plus.<sup>108</sup> The experimental reflection intensities were corrected for absorption using SADABS program.<sup>109</sup> The structures were solved with the ShelXT program<sup>110</sup> and refined by the full-matrix least-squares method (SHELXL-2014)<sup>110</sup> on  $F^2$  over the whole dataset in the anisotropic approximation for all nonhydrogen atoms, both routines being implemented in the Olex2 environment.<sup>111</sup> The Flack parameters of the structures were 0.47 and 0.07 respectively for **Pt6d** and **Pd6d**, which shows possible racemic twinning. The instructions TWIN and BASF were added to ins files and structures were refined again. The refined contributions of racemic twin were 0.470(6) and 0.070(15) respectively for **Pt6d** and **Pd6d**. The hydrogen atoms were placed in the geometrically calculated positions with the isotropic temperature factors set at 1.2 times (CH groups) or 1.5 times (CH<sub>3</sub> group) the equivalent isotropic temperature factor of their bonded C atoms. Table S1† summarizes the crystallographic data and details of the diffraction experiments.

X-ray diffraction experiments were performed at the Center for Shared Use of Physical Methods of Investigation at the Frumkin Institute of Physical Chemistry and Electrochemistry, RAS.

Atomic coordinates have been deposited in the Cambridge Crystallographic Data Centre (the CCDC deposition codes are 2027752 for **Pt6d** and 2027753 for **Pd6d**).†

### Photophysical measurements

Photophysical studies were performed for porphyrin concentrations ranging from 3 to 10  $\mu$ M unless the concentration is not specified in the “Results and discussion” section.

The UV-vis spectra were recorded with a Helios Alpha (Thermo Electron), CARY 50 (Varian), or Jasco V-550 spectrophotometer, using rectangular quartz cells of either 1 or 10 mm optical path length. The ionic strength was adjusted by addition of sodium chloride (NaCl). All solutions were prepared in doubly distilled or deionized water.

Luminescence spectra were recorded on a FluoroLog® 3 spectrofluorometer (Horiba Scientific) equipped with a NIR-sensitive R2658 photomultiplier from Hamamatsu (300–1050 nm). All dye solutions were deoxygenated in a screw-cap cuvette (Hellma) by bubbling high purity nitrogen (99.9999%, Linde Gas, Austria) through the solution for at least 15 min. Absolute quantum yields at room temperature were measured with an integrating sphere from Horiba. The luminescence decay half-times were acquired in the time domain on a FluoroLog® 3 spectrofluorometer equipped with a DeltaHub module (Horiba Scientific) controlling a SpectraLED-392 ( $\lambda$  = 392 nm), using the FluorEssence and the DAS-6 Analysis software for data analysis. Luminescence quenching by molecular oxygen was studied in the same screw-cap cuvette by bubbling gas mixtures through a solution of porphyrin. The composition of the gas mixtures was adjusted with a custom-build gas-mixing device based on mass-flow controllers from Voegtlin (<https://www.red-y.com>) by mixing the test gas (2% of O<sub>2</sub> in N<sub>2</sub>) and nitrogen (99.9999% purity, both from Linde Gas).



### Spectrophotometric titrations

Visible absorption spectra were recorded as a function of pH with a SHIMADZU-2450 spectrophotometer in the 200–800 nm wavelength range. The measurements were performed in a quartz cuvette with an optical path length of 10 mm at  $25 \pm 1$  °C. pH measurements were carried out using a portable Ecotest 2000 pH-meter with a combined ESK-10601/7 glass electrode. All solutions for pH measurements were prepared with deionized water (18.2 M $\Omega$  cm, pH  $\sim$  5.5) produced by a Vodokey cartridge purifier (SPE Himelekttronika, Russia). Protonation studies were conducted in a glass beaker (50 mL), equipped with a magnetic stirrer and pH-electrode. The electrode was calibrated with commercial buffers (pH 1.65, 4.01, and 9.18). Aliquots of 0.1 M HCl were added manually with a Hamilton microsyringe to a porphyrin aqueous solution ( $C = 4.6 \times 10^{-6}$  M) containing sodium chloride ( $C = 0.1$  M). The entire multiwavelength data sets in a pH range of 3.57–10.65 were decomposed into their principal components by factor analysis before adjusting the equilibrium constants and extinction coefficients by nonlinear least-squares analysis with the HypSpec program.<sup>112</sup>

### Photophysical studies of the singlet oxygen generation chemical trapping method

The methodology followed in this study was based on our previously published works.<sup>106</sup> Briefly, freshly prepared stock solutions of 1,9-anthracenedipropionic acid (ADPA) and the PS under investigation (1 mL of each, dissolved in MeCN/H<sub>2</sub>O (4:1 v/v)) were placed in a 3.5 mL quartz cuvette (Hellma, 100-QS, 45  $\times$  12.5  $\times$  12.5 mm, light path 10 mm) and stirred at 200 rpm throughout the irradiation period. The concentration of each solution was adjusted to ensure equal absorbance ( $A = 0.1$ ) for both the PS and ADPA at the irradiation wavelength. A control experiment was conducted using ADPA diluted twice (without an exogenous PS), serving as a blank with identical absorbance to the ADPA in the other samples. All studied solutions were irradiated using the xenon arc lamp from the spectrofluorometer, with the irradiation wavelength centered between 397 and 400 nm, depending on the experiment. The entrance slits were set at 5 nm, ensuring a constant irradiation power of 5 mW across all experiments. Details of the calculation of PS quantum yield from first-order linearization of the three curves (PH + ADPA, ADPA alone, and PS + ADPA) are provided elsewhere.<sup>106</sup> The graphs obtained from these studies are presented in the ESI (Fig. S31–S36†).

### Estimation of singlet oxygen generation using the EPR technique

4-oxo-TEMP (TCI), phenalenone (PH) (Merck) and Rose Bengal (Acros) were used as received. Quantitative studies were conducted to assess the amount of singlet oxygen generated by Pd3d or PdTCPP utilizing 4-oxo-TEMP as a spin trap in aqueous solutions, in comparison with PH or Rose Bengal, dissolved in the same solvents. A set of three solutions, each with

an equal absorption value ( $A = 0.068$ ) at 365 nm, was meticulously prepared by dissolving metalloporphyrins and PH in water (Thermo Scientific, Spectrophotometric grade). Following this, 25 mM solutions of 4-oxo-TEMP in the same solvent were prepared, and equivalent volumes (250  $\mu$ L) of chromophore and 4-oxo-TEMP solutions were mixed in a glass vial. The resulting solution was then transferred to a quartz precision EPR tube and promptly examined using EPR spectroscopy. Measurements were performed *in situ* under photoexcitation in a standard EPR cavity on a X-band Bruker spectrometer equipped with a 365 nm LED (Thorlab),<sup>113</sup> with irradiation times ranging from 0 to 15 min. These EPR assays were carried out at room temperature, with settings including a modulation frequency of 100 kHz, a microwave power of 7 mW (365 nm) or 23 mW (530 nm), a modulation amplitude of 1 G, a time constant of 20.5 ms, and a single acquisition scan. The temporal change in 4-oxo-TEMP concentration with time was plotted. The data were not subjected to further analysis, as the rate of singlet oxygen generation by PH was significantly lower than those of Pd3d and PdTCPP, despite the expected  $\Phi_{\Delta} = 1$  for this compound.<sup>114</sup>

The second set of three solutions, each with an equal absorption value ( $A = 0.4$ ) at 530 nm, was prepared by dissolving metalloporphyrins and Rose Bengal in water. The measurements were conducted using the same procedure but using a 530 nm LED (Thorlab). The temporal change in 4-oxo-TEMP concentration with time was plotted (Fig. S29†) and the singlet oxygen quantum yields ( $\Phi_{\Delta}$ ) were determined using the reported values for Rose Bengal ( $\Phi_{\Delta} = 0.75$ ).<sup>85</sup>

### Photostability studies

Photostability measurements in buffered H<sub>2</sub>O/DMF were performed on a set-up described previously.<sup>61</sup> They were conducted in a 100 mL double-jacketed glass vessel equipped with a magnetic stirring bar, a thermometer, and an immersion probe with a 10 mm optical path length made from Suprasil 300 (Hellma). The vessel was fitted to a Lauda RE106 water circulator ensuring a constant temperature of  $25.0 \pm 5$  °C. The probe was connected to a Cary 50 (Varian) spectrophotometer through fiber guides and a fiber optic coupler. Visible absorption spectra were recorded over the 350–800 nm range. Kinetic traces were recorded at the maximum of the Soret band with an average time of 0.1 s by taking one point every minute until the end of the reaction (typically, 5000–7000 min). The light source was an Osram Powerstat HQI BT 400 W lamp (metal halogenide lamp with UV filter) and was placed in a fixed position 20 cm away from the glass reactor. The data obtained are presented in Fig. 8.

Photostability measurements in MeCN/H<sub>2</sub>O were performed using a Jasco V-550 spectrophotometer in a rectangular quartz cell (Hellma, 100-QS, 45  $\times$  12.5  $\times$  12.5 mm, 10 mm optical path length, chamber volume 3.5 mL). Isoabsorbing solutions of the studied compounds were prepared, placed in closed vials, and irradiated in the EvoluChem Photoredox box using a blue LED (425 nm, 18 W). The spectra recorded after 3 h of irradiation are presented in Fig. S38.†

### Photocatalytic oxidation of sulfides

Aqueous solutions of porphyrins (0.01 M) were prepared in 5 mL volumetric flasks. The weighed amount of **Pd2d**, **Pd3d**, or **PdTCPP** was dissolved with 40–200  $\mu\text{L}$  of 0.1 M aqueous NaOH before the flask was filled with deionized water.

### General procedure of sulfoxidation in the presence of **Pd2d**, **Pd3d**, or **PdTCPP**

An 8 mL microwave tube equipped with a magnetic stirring bar was sealed with a silicone septum and filled with pure oxygen by performing three cycles of evacuation and oxygen purging. The tube was equipped with a 1 L balloon filled with oxygen and charged with 0.5 mmol of sulfide (see Table 1) along with the calculated amount of a standard photocatalyst solution (to obtain 0.025 mol% of the photocatalyst). Then water (0.5 mL) and MeCN (to obtain 2 mL in the reaction mixture) were added. The reaction tube was irradiated with a blue LED (425 nm, 18 W) and stirred in a EvoluChem Photoredox box. When the reaction was complete (monitoring by NMR), the mixture was diluted with 7 mL of water and extracted with dichloromethane ( $3 \times 5$  mL). The combined organic phases were dried over sodium sulfate and evaporated under reduced pressure at room temperature. The yield and purity of the products were determined by  $^1\text{H}$  NMR spectroscopy using biphenyl as an internal standard. The reaction times and the product yields are provided in Scheme 2 and Table S7.†

This catalyst loading was also used in the kinetic studies (Table S7†) which were performed using the same procedure. The reactions were periodically monitored by NMR spectroscopy after withdrawing aliquot samples.

The experiments with the recycled photocatalyst were performed using the same procedure in a MeCN/ $\text{H}_2\text{O}$  mixture (2.5 mL, 1 : 1 v/v) using 0.05 mol% of **Pd3d**. After completion of the reaction, the product was extracted with  $\text{CH}_2\text{Cl}_2$  ( $3 \times 5$  mL) and the aqueous phase (pH 7–8) containing the photocatalyst was introduced in the next catalytic cycle.

### Author contributions

M. V. V. synthesized and characterized the porphyrins, performed the aggregation studies and photophysical measurements, wrote the corresponding sections, and prepared TOC. G. A. K. conducted VT NMR studies and wrote the corresponding section. A. A. S. was responsible for single-crystal X-ray characterization and wrote the corresponding section. Yu. G. G. and A. Yu. T. were responsible for funding acquisition and supervision, and participated in editing. E. V. E. was involved in the titration experiments. M. M. performed the photodegradation studies, guided the interpretation of titration experiments, wrote the corresponding sections, and edited the manuscript. C. M. studied the singlet oxygen generation by fluorescence spectroscopy and wrote the corresponding section. S. M. B. supervised the luminescence studies and oxygen-quenching experiments and wrote the corres-

ponding section. L. K. and S. P. conducted EPR studies and wrote that section. A. B.-L. was responsible for project conceptualization, performed the synthesis of porphyrins, studied the photocatalytic properties, wrote these sections and edited the manuscript.

### Data availability

All important data supporting this article have been included in the ESI.†

### Conflicts of interest

There are no conflicts to declare.

### Acknowledgements

This work was supported by the Ministry of Science and Higher Education of Russian Federation, the Russian Science Foundation (grant No. 24-73-10227), the Russian Academy of Sciences (RAS), the Centre National de la Recherche Scientifique (CNRS), and l'Ecole Normale Supérieure de Lyon (ENS de Lyon). It was started in the framework of the International Associated French–Russian Laboratory of Macrocyclic Systems and Related Materials (LAMREM) of CNRS.

### References

- 1 M. Ethirajan, Y. Chen, P. Joshi and R. K. Pandey, *Chem. Soc. Rev.*, 2011, **40**, 340–362.
- 2 A. Akbar, S. Khan, T. Chatterjee and M. Ghosh, *J. Photochem. Photobiol., B*, 2023, **248**, 112796.
- 3 J. F. Lovell, T. W. B. Liu, J. Chen and G. Zheng, *Chem. Rev.*, 2010, **110**, 2839–2857.
- 4 T. Lee, X.-A. Zhang, S. Dhar, H. Faas, S. J. Lippard and A. Jasanoff, *Chem. Biol.*, 2010, **17**, 665–673.
- 5 A. M. Amado, J. H. Uliana, T. Z. Pavan and I. Borissevitch, *Chem. Phys. Lett.*, 2020, **738**, 136875.
- 6 M. Luciano, M. Erfanzadeh, F. Zhou, H. Zhu, T. Bornhütter, B. Röder, Q. Zhu and C. Brückner, *Org. Biomol. Chem.*, 2017, **15**, 972–983.
- 7 R. Gerdes, D. Wöhrle, W. Spiller, G. Schneider, G. Schnurpfeil and G. Schulz-Ekloff, *J. Photochem. Photobiol., A*, 1997, **111**, 65–74.
- 8 M. L. Marin, L. Santos-Juanes, A. Arques, A. M. Amat and M. A. Miranda, *Chem. Rev.*, 2012, **112**, 1710–1750.
- 9 E. Giannoudis, E. Benazzi, J. Karlsson, G. Copley, S. Panagiotakis, G. Landrou, P. Angaridis, V. Nikolaou, C. Matthaiaki, G. Charalambidis, E. A. Gibson and A. G. Coutsolelos, *Inorg. Chem.*, 2020, **59**, 1611–1621.
- 10 I. D. Kostas, A. G. Coutsolelos, G. Charalambidis and A. Skondra, *Tetrahedron Lett.*, 2007, **48**, 6688–6691.

- 11 H.-C. Chen, D. G. H. Hetterscheid, R. M. Williams, J. I. van der Vlugt, J. N. H. Reek and A. M. Brouwer, *Energy Environ. Sci.*, 2015, **8**, 975–982.
- 12 K. U. Rao, J. Lakshmidevi, R. M. Appa, S. S. Prasad, M. Narasimhulu, R. Vijitha, K. S. V. K. Rao and K. Venkateswarlu, *ChemistrySelect*, 2017, **2**, 7394–7398.
- 13 K. U. Rao and K. Venkateswarlu, *Synlett*, 2018, 1055–1060.
- 14 Q.-X. Wan and Y. Liu, *Catal. Lett.*, 2009, **128**, 487–492.
- 15 J. F. Lovell, A. Roxin, K. K. Ng, Q. Qi, J. D. McMullen, R. S. DaCosta and G. Zheng, *Biomacromolecules*, 2011, **12**, 3115–3118.
- 16 F. Giuntini, V. M. Chauhan, J. W. Aylott, G. A. Rosser, A. Athanasiadis, A. Beeby, A. J. MacRobert, R. A. Brown and R. W. Boyle, *Photochem. Photobiol. Sci.*, 2014, **13**, 1039–1051.
- 17 Z.-A. Chen, Y. Kuthati, R. K. Kankala, Y.-C. Chang, C.-L. Liu, C.-F. Weng, C.-Y. Mou and C.-H. Lee, *Sci. Technol. Adv. Mater.*, 2015, **16**, 054205.
- 18 V. V. Vasil'ev and S. M. Borisov, *Sens. Actuators, B*, 2002, **82**, 272–276.
- 19 H.-G. Jeong and M.-S. Choi, *Isr. J. Chem.*, 2016, **56**, 110–118.
- 20 J. Roales, J. M. Pedrosa, P. Castillero, M. Cano, T. H. Richardson, Á. Barranco and A. R. González-Elipe, *ACS Appl. Mater. Interfaces*, 2012, **4**, 5147–5154.
- 21 S. Afzal, W. A. Daoud and S. J. Langford, *J. Mater. Chem.*, 2012, **22**, 4083–4088.
- 22 L. Feng, K.-Y. Wang, E. Joseph and H.-C. Zhou, *Trends Chem.*, 2020, **2**, 555–568.
- 23 X. Zhang, M. C. Wasson, M. Shayan, E. K. Berdichevsky, J. Ricardo-Noordberg, Z. Singh, E. K. Papazyan, A. J. Castro, P. Marino, Z. Ajoyan, Z. Chen, T. Islamoglu, A. J. Howarth, Y. Liu, M. B. Majewski, M. J. Katz, J. E. Mondloch and O. K. Farha, *Coord. Chem. Rev.*, 2021, **429**, 213615.
- 24 F. G. Moscoso, J. J. Romero-Guerrero, D. Rodriguez-Lucena, J. M. Pedrosa and C. Carrillo-Carrión, *Small Sci.*, 2024, **4**, 2400210.
- 25 A. D. G. Firmino, F. Figueira, J. P. C. Tomé, F. A. A. Paz and J. Rocha, *Coord. Chem. Rev.*, 2018, **355**, 133–149.
- 26 Y. Y. Enakieva, A. A. Sinelshchikova, M. S. Grigoriev, V. V. Chernyshev, K. A. Kovalenko, I. A. Stenina, A. B. Yaroslavtsev, Y. G. Gorbunova and A. Y. Tsivadze, *Chem. – Eur. J.*, 2019, **25**, 10552–10556.
- 27 M.-H. Xie, X.-L. Yang and C.-D. Wu, *Chem. Commun.*, 2011, **47**, 5521–5523.
- 28 G. Rana, P. Dhiman, A. Kumar, T. Wang and G. Sharma, *Chem. Eng. Res. Des.*, 2023, **199**, 620–638.
- 29 F. Liu, I. Rincón, H. G. Baldoví, A. Dhakshinamoorthy, P. Horcajada, S. Rojas, S. Navalón and A. Fateeva, *Inorg. Chem. Front.*, 2024, **11**, 2212–2245.
- 30 G. Simonneaux, P. Le Maux, S. Chevance and H. Srou, in *Handbook of Porphyrin Science*, ed. K. M. Kadish, K. M. Smith and R. Guilard, World Scientific, Singapore, 2012, vol. 21, pp. 377–410.
- 31 R. H. Schmehl and D. G. Whitten, *J. Phys. Chem.*, 1981, **85**, 3473–3480.
- 32 C. Tanielian and G. Heinrich, *Photochem. Photobiol.*, 1995, **61**, 131–135.
- 33 C. Tanielian, C. Wolff and M. Esch, *J. Phys. Chem.*, 1996, **100**, 6555–6560.
- 34 S. Singh, A. Aggarwal, N. V. S. D. K. Bhupathiraju, G. Arianna, K. Tiwari and C. M. Drain, *Chem. Rev.*, 2015, **115**, 10261–10306.
- 35 J. N. Silva, F. Bosca, J. P. C. Tomé, E. M. P. Silva, M. G. P. M. S. Neves, J. A. S. Cavaleiro, L. K. Patterson, P. Filipe, J.-C. Mazière, R. Santus and P. Morlière, *J. Phys. Chem. B*, 2009, **113**, 16695–16704.
- 36 D. Lazewski, M. Kucinska, E. Potaptskiy, J. Kuzminska, A. Tezyk, L. Popenda, S. Jurga, A. Teubert, Z. Gdaniec, J. Kujawski, K. Grzyb, T. Pedzinski, M. Murias and M. Wierzchowski, *Int. J. Mol. Sci.*, 2022, **23**, 10029.
- 37 B. W. Pedersen, L. E. Sinks, T. Breitenbach, N. B. Schack, S. A. Vinogradov and P. R. Ogilby, *Photochem. Photobiol.*, 2011, **87**, 1077–1091.
- 38 M. Tang, Y. Song, Y.-L. Lu, Y.-M. Zhang, Z. Yu, X. Xu and Y. Liu, *J. Med. Chem.*, 2022, **65**, 6764–6774.
- 39 R. W. Redmond, *Photochem. Photobiol.*, 1991, **54**, 547–556.
- 40 A. M. Master, M. E. Rodriguez, M. E. Kenney, N. L. Oleinick and A. S. Gupta, *J. Pharm. Sci.*, 2010, **99**, 2386–2398.
- 41 B. F. O. Nascimento, N. A. M. Pereira, A. J. M. Valente, T. M. V. D. Pinho e Melo and M. Pineiro, *Pharmaceutics*, 2019, **11**, 81.
- 42 J. Xie, Y. Wang, W. Choi, P. Jangili, Y. Ge, Y. Xu, J. Kang, L. Liu, B. Zhang, Z. Xie, J. He, N. Xie, G. Nie, H. Zhang and J. S. Kim, *Chem. Soc. Rev.*, 2021, **50**, 9152–9201.
- 43 Y. Matano, K. Matsumoto, Y. Terasaka, H. Hotta, Y. Araki, O. Ito, M. Shiro, T. Sasamori, N. Tokitoh and H. Imahori, *Chem. – Eur. J.*, 2007, **13**, 891–901.
- 44 Y. Y. Enakieva, A. G. Bessmertnykh, Y. G. Gorbunova, C. Stern, Y. Rousselin, A. Y. Tsivadze and R. Guilard, *Org. Lett.*, 2009, **11**, 3842–3845.
- 45 Y. Y. Enakieva, J. Michalak, I. A. Abdulaeva, M. V. Volostnykh, C. Stern, R. Guilard, A. G. Bessmertnykh-Lemeune, Y. G. Gorbunova, A. Y. Tsivadze and K. M. Kadish, *Eur. J. Org. Chem.*, 2016, 4881–4892.
- 46 E. V. Vinogradova, Y. Y. Enakieva, S. E. Nefedov, K. P. Birin, A. Y. Tsivadze, Y. G. Gorbunova, A. G. Bessmertnykh-Lemeune, C. Stern and R. Guilard, *Chem. – Eur. J.*, 2012, **18**, 15092–15104.
- 47 Y. Y. Enakieva, M. V. Volostnykh, S. E. Nefedov, G. A. Kirakosyan, Y. G. Gorbunova, A. Y. Tsivadze, A. G. Bessmertnykh-Lemeune, C. Stern and R. Guilard, *Inorg. Chem.*, 2017, **56**, 3055–3070.
- 48 Y.-S. Kim, S. Kriegel, A. Bessmertnykh-Lemeune, K. D. Harris, B. Limoges and V. Balland, *ChemElectroChem*, 2021, **8**, 2640–2648.
- 49 D. B. Papkovsky and T. C. O'Riordan, *J. Fluoresc.*, 2005, **15**, 569–584.
- 50 M. Yang, J. Deng, D. Guo, J. Zhang, L. Yang and F. Wu, *Org. Biomol. Chem.*, 2019, **17**, 5367–5374.

- 51 Y. Amao, *Microchim. Acta*, 2003, **143**, 1–12.
- 52 X. Chen, X. Tian, I. Shin and J. Yoon, *Chem. Soc. Rev.*, 2011, **40**, 4783–4804.
- 53 X.-D. Wang and O. S. Wolfbeis, *Chem. Soc. Rev.*, 2014, **43**, 3666–3761.
- 54 D. R. Subedi, R. Reid, P. F. D'Souza, V. N. Nesterov and F. D'Souza, *ChemPlusChem*, 2022, **87**, e202200010.
- 55 Y. Vakrat-Haglil, L. Weiner, V. Brumfeld, A. Brandis, Y. Salomon, B. McLlroy, B. C. Wilson, A. Pawlak, M. Rozanowska, T. Sarna and A. Scherz, *J. Am. Chem. Soc.*, 2005, **127**, 6487–6497.
- 56 I. Ashur, R. Goldschmidt, I. Pinkas, Y. Salomon, G. Szweczyk, T. Sarna and A. Scherz, *J. Phys. Chem. A*, 2009, **113**, 8027–8037.
- 57 O. S. Finikova, A. Y. Lebedev, A. Aprelev, T. Troxler, F. Gao, C. Garnacho, S. Muro, R. M. Hochstrasser and S. A. Vinogradov, *ChemPhysChem*, 2008, **9**, 1673–1679.
- 58 L. E. Sinks, G. P. Robbins, E. Roussakis, T. Troxler, D. A. Hammer and S. A. Vinogradov, *J. Phys. Chem. B*, 2010, **114**, 14373–14382.
- 59 A. Lascu, *ARKIVOC*, 2020, **2020**, 272–296.
- 60 P. Tholen, C. A. Peeples, M. M. Ayhan, L. Wagner, H. Thomas, P. Imbrasas, Y. Zorlu, C. Baretzky, S. Reineke, G. Hanna and G. Yücesan, *Small*, 2022, **18**, 2204578.
- 61 M. V. Volostnykh, S. M. Borisov, M. A. Konovalov, A. A. Sinelshchikova, Y. G. Gorbunova, A. Y. Tsivadze, M. Meyer, C. Stern and A. Bessmertnykh-Lemeune, *Dalton Trans.*, 2019, **48**, 8882–8898.
- 62 E. B. Fleischer, C. K. Miller and L. E. Webb, *J. Am. Chem. Soc.*, 1964, **86**, 2342–2347.
- 63 M. Shmilovits, M. Vinodu and I. Goldberg, *Cryst. Growth Des.*, 2004, **4**, 633–638.
- 64 W. Wu, W. Wu, S. Ji, H. Guo, X. Wang and J. Zhao, *Dyes Pigm.*, 2011, **89**, 199–211.
- 65 R. I. Zubatyuk, A. A. Sinelshchikova, Y. Y. Enakieva, Y. G. Gorbunova, A. Y. Tsivadze, S. E. Nefedov, A. Bessmertnykh-Lemeune, R. Guilard and O. V. Shishkin, *CrystEngComm*, 2014, **16**, 10428–10438.
- 66 A. Albinati, F. Lianza, P. S. Pregosin and B. Mueller, *Inorg. Chem.*, 1994, **33**, 2522–2526.
- 67 A. N. Vedernikov, M. Pink and K. G. Caulton, *Inorg. Chem.*, 2004, **43**, 3642–3646.
- 68 S. Chatterjee, J. A. Krause, A. G. Oliver and W. B. Connick, *Inorg. Chem.*, 2010, **49**, 9798–9808.
- 69 A. Behnia, M. A. Fard, P. D. Boyle and R. J. Puddephatt, *Eur. J. Inorg. Chem.*, 2019, **2019**, 2899–2906.
- 70 P. Ristić, V. Blagojević, G. Janjić, M. Rodić, P. Vulić, M. Donnard, M. Gulea, A. Chylewska, M. Makowski, T. Todorović and N. Filipović, *Cryst. Growth Des.*, 2020, **20**, 3018–3033.
- 71 K. Bütje and K. Nakamoto, *Inorg. Chim. Acta*, 1990, **167**, 97–108.
- 72 K. Shinozaki, K. Miwa, H. Yokoyama and H. Matsuzawa, *J. Chem. Soc., Faraday Trans.*, 1996, **92**, 1935–1939.
- 73 V. V. Vasil'ev, S. M. Borisov and Y. O. Chubarova, *Russ. J. Inorg. Chem.*, 2003, **48**, 385–390.
- 74 K. Kalyanasundaram and M. Neumann-Spallart, *J. Phys. Chem.*, 1982, **86**, 5163–5169.
- 75 S. A. Vinogradov and D. F. Wilson, *J. Chem. Soc., Perkin Trans. 2*, 1995, 103–111.
- 76 I. A. Blinova and V. V. Vasil'ev, *Russ. J. Phys. Chem.*, 1995, **69**, 995–999.
- 77 R. F. Pasternack, P. R. Huber, P. Boyd, G. Engasser, L. Francesconi, E. Gibbs, P. Fasella, G. Cerio Venturo and L. deC Hinds, *J. Am. Chem. Soc.*, 1972, **94**, 4511–4517.
- 78 H. Ozeki, A. Nomoto, K. Ogawa, Y. Kobuke, M. Murakami, K. Hosoda, M. Ohtani, S. Nakashima, H. Miyasaka and T. Okada, *Chem. – Eur. J.*, 2004, **10**, 6393–6401.
- 79 K. Kano, H. Minamizono, T. Kitae and S. Negi, *J. Phys. Chem. A*, 1997, **101**, 6118–6124.
- 80 A. E. Martell, R. M. Smith and R. J. Motekaitis, in *NIST Standard Reference Database*, Gaithersburg, MD, 2004, vol. 46.
- 81 J. B. Callis, J. M. Knowles and M. Gouterman, *J. Phys. Chem.*, 1973, **77**, 154–157.
- 82 S. M. Borisov and V. V. Vasil'ev, *Russ. J. Phys. Chem.*, 1994, **75**, 1890–1895.
- 83 S. M. Borisov, PhD thesis, Saint Petersburg, Russia, 2003. <https://www.dissercat.com/content/perenos-energii-elektronnogo-vozbuzhdeniya-i-generatsiya-singletnogo-kislorda-kompleksami-p>.
- 84 G. Nardi, I. Manet, S. Monti, M. A. Miranda and V. Lhiaubet-Vallet, *Free Radicals Biol. Med.*, 2014, **77**, 64–70.
- 85 E. Gandin, Y. Lion and A. Van de Vorst, *Photochem. Photobiol.*, 1983, **37**, 271–278.
- 86 S. M. Borisov, I. A. Blinova and V. V. Vasil'ev, *High Energy Chem.*, 2002, **36**, 189–192.
- 87 J. M. Fernandez, M. D. Bilgin and L. I. Grossweiner, *J. Photochem. Photobiol., B*, 1997, **37**, 131–140.
- 88 T. Nishimura, K. Hara, N. Honda, S. Okazaki, H. Hazama and K. Awazu, *Lasers Med. Sci.*, 2020, **35**, 1289–1297.
- 89 Q. Zheng and L. D. Lavis, *Curr. Opin. Chem. Biol.*, 2017, **39**, 32–38.
- 90 S.-K. Lee and I. Okura, *Anal. Commun.*, 1997, **34**, 185–188.
- 91 S.-W. Lai, Y.-J. Hou, C.-M. Che, H.-L. Pang, K.-Y. Wong, C. K. Chang and N. Zhu, *Inorg. Chem.*, 2004, **43**, 3724–3732.
- 92 P. E. Ellis and J. E. Lyons, *J. Chem. Soc., Chem. Commun.*, 1989, 1315–1316.
- 93 A. G. Mojarad and S. Zakavi, *Catal. Sci. Technol.*, 2018, **8**, 768–781.
- 94 R. Costa e Silva, L. Oliveira da Silva, A. de Andrade Bartolomeu, T. J. Brocksom and K. T. de Oliveira, *Beilstein J. Org. Chem.*, 2020, **16**, 917–955.
- 95 E. Baciocchi, T. Del Giacco, O. Lanzalunga, P. Mencarelli and B. Procacci, *J. Org. Chem.*, 2008, **73**, 5675–5682.
- 96 S. Matavos-Aramyan, S. Soukhakian and M. H. Jazebizadeh, *Phosphorus, Sulfur Silicon Relat. Elem.*, 2020, **195**, 181–193.
- 97 A. Sheldon, *Metalloporphyrins in Catalytic Oxidations*, Marcel Dekker, New York, 1994.



- 98 N. A. Stephenson and A. T. Bell, *J. Mol. Catal. A: Chem.*, 2007, **272**, 108–117.
- 99 G. da Silva, S. M. G. Pires, V. L. M. Silva, M. M. Q. Simões, M. G. P. M. S. Neves, S. L. H. Rebelo, A. M. S. Silva and J. A. S. Cavaleiro, *Catal. Commun.*, 2014, **56**, 68–71.
- 100 T. Neveselý, E. Svobodová, J. Chudoba, M. Sikorski and R. Cibulka, *Adv. Synth. Catal.*, 2016, **358**, 1654–1663.
- 101 M. Bettoni, T. Del Giacco, M. Stradiotto and F. Elisei, *J. Org. Chem.*, 2015, **80**, 8001–8008.
- 102 G. V. Morozkov, A. S. Abel, M. A. Filatov, S. E. Nefedov, V. A. Roznyatovsky, A. V. Cheprakov, A. Y. Mitrofanov, I. S. Ziankou, A. D. Averin, I. P. Beletskaya, J. Michalak, C. Bucher, L. Bonneviot and A. Bessmertnykh-Lemeune, *Dalton Trans.*, 2022, **51**, 13612–13630.
- 103 E. Baciocchi, T. D. Giacco, F. Elisei, M. F. Gerini, M. Guerra, A. Lapi and P. Liberali, *J. Am. Chem. Soc.*, 2003, **125**, 16444–16454.
- 104 S. M. Bonesi, I. Manet, M. Freccero, M. Fagnoni and A. Albini, *Chem. – Eur. J.*, 2006, **12**, 4844–4857.
- 105 E. L. Clennan, *Acc. Chem. Res.*, 2001, **34**, 875–884.
- 106 M. Galland, T. Le Bahers, A. Banyasz, N. Lascoux, A. Duperray, A. Grichine, R. Tripier, Y. Guyot, M. Maynadier, C. Nguyen, M. Gary-Bobo, C. Andraud, C. Monnereau and O. Maury, *Chem. – Eur. J.*, 2019, **25**, 9026–9034.
- 107 K. El-Naggar, H. S. Abdel-Samad, R. M. Ramadan, M. E. El-Khouly and A. A. Abdel-Shafi, *J. Photochem. Photobiol., A*, 2023, **436**, 114405.
- 108 Bruker (after 2019), *SAINT-Plus*, Bruker AXS Inc., Madison, Wisconsin, USA.
- 109 Bruker (after 2013), *SADABS*, Bruker AXS Inc., Madison, Wisconsin, USA.
- 110 G. Sheldrick, *Acta Crystallogr., Sect. C: Struct. Chem.*, 2015, **71**, 3–8.
- 111 O. V. Dolomanov, L. J. Bourhis, R. J. Gildea, J. A. K. Howard and H. Puschmann, *J. Appl. Crystallogr.*, 2009, **42**, 339–341.
- 112 P. Gans, *HypSpec2014*, Protonic Software, UK, <https://www.hyperquad.co.uk/HypSpec2014.htm> (accessed Nov. 2024).
- 113 C. Mendoza, A. Désert, L. Khrouz, C. A. Páez, S. Parola and B. Heinrichs, *Environ. Sci. Pollut. Res.*, 2021, **28**, 25124–25129.
- 114 R. Schmidt, C. Tanielian, R. Dunsbach and C. Wolff, *J. Photochem. Photobiol., A*, 1994, **79**, 11–17.